

Integration of Remote Sensing and Risk Analysis for Airframe Structural Integrity Assessment

D. Cope¹, J. Cronenberger¹, K. Kozak¹, K. Schrader¹,
L. Smith¹, and C. Thwing¹

¹ Southwest Research Institute, San Antonio, Texas, 78238, USA

dale.cope@swri.org

jody.cronenberger@swri.org

kris.kozak@swri.org

kurt.schrader@swri.org

luciano.smith@swri.org

clinton.thwing@swri.org

ABSTRACT

Southwest Research Institute (SwRI) investigated the feasibility of integrating remote sensing technology with probability of failure analyses into a monitoring system capable of assessing the structural integrity of critical airframe components. The project demonstrated the viability of remote sensing to discern structural flaw growth along with the integration of sensor data with crack growth analyses in order to assess the health and integrity of a critical structural component. The demonstration was performed on a complicated aircraft structural component that has limited accessibility with realistic loading. The technical approach employed for developing the structural health monitoring system included (1) detailed stress analyses of a critical structural component, (2) crack growth analyses to predict the structural component's fatigue life, (3) a damage sensor system to monitor the structural components and capture degradation mechanisms during fatigue testing, (4) reasoning algorithms to integrate damage sensor data with crack growth analyses in order to assess the current structural health and integrity of the component, and (5) predictions of the component's structural capability and remaining useful life on a periodic basis. Researchers used Bayesian principles to estimate flaw sizes based on both sensor readings and crack growth analyses, which were then used for periodic structural health and integrity assessments. Results validated how fatigue life predictions and probability of failure assessments can be improved with more accurate estimates of actual flaw sizes and continual structural health monitoring.*

* This is an open-access article distributed under the terms of the Creative Commons Attribution 3.0 United States License, which permits unrestricted use, distribution, and reproduction in any medium, provided the original author and source are credited.

1. INTRODUCTION

Recent technology developments in structural damage detection methods and usage monitoring of aircraft structures holds the promise of assuring the safety and operational readiness of the nation's military and civilian aircraft fleets. This promise can be fulfilled through effective damage assessment of critical safety-of-flight (SOF) structures that are inaccessible. For the military, the situation today is that a large number of aging aircraft are in fleet inventory and have to be maintained in an acceptable state of operational readiness (Giurgiutiu, 2007). This situation is likely to persist for some time. For commercial aviation, the future increase in aviation traffic and new forms of aircraft will create an increasingly complex aviation environment that must also safely operate with older assets. Entire suites of new safety technologies must be introduced if this increased complexity of aviation operations is to be achieved safely (Aeronautics Science and Technology Subcommittee, 2007)

One of the aviation safety goals in the National Plan for Aeronautics Research and Development (R&D) is to develop technologies to reduce accidents and incidents through enhanced vehicle design, structure, and subsystems. A near-term objective of this goal is the development of vehicle health-management systems to determine the state of degradation for aircraft subsystems (Aeronautics Science and Technology Subcommittee, 2007). For the airframe subsystem, promising technology includes on-board sensors for damage detection and real-time monitoring of aircraft flight parameters. Integration of these two technology areas would significantly advance the diagnostics and prognostics capabilities for assessing critical SOF structural components. These advances would provide continued improvement in aviation safety while also reducing the burden of traditional detecting and

identifying structural damage, thereby increasing maintenance effectiveness, reducing downtime, and increasing aircraft availability.

1.1 Technical Background

Identification and Significance of Problem The continued operation of aging aircraft increases the risk of catastrophic failure of critical components and increases the economic costs for insuring the continued airworthiness. The increased capability and complexity of newer vehicles creates greater challenges for performing safety inspections of structures and system components that operate under more severe usage environments (Hudak et al., 2006). Even though aviation is applauded for its outstanding safety record and well-established procedures exist to detect the effects of structural damage, recent and unanticipated failures of aircraft structures have compelled the engineering community to re-examine design philosophies and inspection practices for insuring continued airworthiness (Roach, 2007). Under the inspection-based damage tolerant design philosophy for aircraft structure, safety inspections are designed to detect cracks that potentially exist at known cracking locations (Gallagher, 2007). This design philosophy requires that a structure be capable of sustaining small damage without failure and that a nondestructive inspection (NDI) program be instituted to detect such flaws before they grow to critical size. This approach emphasizes inspection to ensure safety and reliability; however, recent events, such as increased number of cracking sites and larger crack sizes found at some sites in aging airframes, along with numerous cracks missed during inspections, have shaken engineers' confidence in this design philosophy (Gallagher, 2007). These recent "surprises" and "near misses" have shown that the reliability of current NDI is not adequate for ensuring safety, thereby increasing structural and aircraft systems risk while decreasing aircraft availability (Hatcher, 2007).

The criticality of insuring the structural integrity of critical SOF components is highlighted by four high-profile mishaps over a period of six years. The first extreme example of this shortfall in aviation safety is the crash of a C-130A on June 17, 2002. This aircraft was operating within a normal firefighting mission profile when its wings separated in flight, resulting in three fatalities. During the crash investigation, a twelve inch fatigue crack was discovered underneath a doubler (Hatcher, 2007). A similar mishap occurred just one month later on a Vultee P4Y aircraft, resulting in two fatalities. This aircraft had extensive areas of preexisting fatigue in the left wing's forward spar lower spar cap, the adjacent spar web, and the adjacent area of the lower wing skin.

A third high-profile mishap due to structural failure occurred on December 19, 2005 when the left wing on a Grumman G-73T Mallard separated from the aircraft in flight, resulting in twenty fatalities. The accident investigation found evidence of fatigue cracking in the lower rear wing spar cap, along the lower wing skin, and on an internal z-stringer with additional evidence of fatigue cracking in the corresponding area on the left wing. The fourth extreme example is the more recent crash of an F-15C on November 2, 2007. The aircraft was conducting basic fighter maneuvers when the forward fuselage broke apart from the aft portion of the aircraft. The accident investigation identified a fatigue crack in the upper cockpit longeron, which led to longeron failure and subsequent breakup of the aircraft, which is shown in the animation in Figure 1. Prior to the mishap event, no inspection criteria existed for detecting a crack in the longeron since this structure did not show any cracking issues during initial fatigue testing on the aircraft (Wignall, 2007). While the fatigue cracking in each of these mishaps could have been detected by conventional NDI methods before reaching critical length, the reliance on existing inspection procedures failed to ensure the integrity of the aircraft structure and the safety of the aircrew and passengers.



Figure 1: Aircraft Mishap Resulting from Catastrophic Structural Failure

Current Technology Conventional NDI techniques, such as eddy-current, ultrasound, radiography, thermography, etc., are used to examine a material for geometry, damage or composition by using technology that does not negatively affect the structure's future usefulness. These techniques involve the use of discrete testing devices that must be in contact with or adjacent to the surface of the structure at the flaw location. These inspections require that the aircraft be on the ground and typically only cover a local area of the structure (Roach, 2007). They are limited to certain kinds of materials and structural geometries, and they usually require a skilled technician to interpret the observations. Inspection technicians often have

difficulties in quantifying the damage. Adequate access to certain structures may require expensive and time-consuming disassembly, which increase labor costs and add to the time needed to complete the inspection. Disassembly of inaccessible areas may also induce additional damage in critical structure. Innovative techniques and damage detection technology are needed to avoid some of the current limitations in NDI and to ensure the integrity of critical SOF structure in today's aging military and civilian aircraft along with tomorrow's more complex air vehicles.

Advances in speed, data storage, and channel capacity of flight data recorders are providing increased capabilities in actual usage monitoring on many military and civilian aircraft. Current capabilities include the measurement and recording of operational parameters during each flight, which can subsequently be used to identify and establish flight regimes that are indicative of the actual structural flight loads experienced by the aircraft. However, current fleet tracking programs only review recorded flight data off the aircraft after periodic downloads. Post-flight analysis of flight data is used to estimate remaining fatigue life, and damage tolerance analyses of fatigue critical areas are updated based on actual usage in order to establish inspection and maintenance intervals for these areas.

In contrast to conventional NDI techniques and usage monitoring methods, the capability exists in current technologies to integrate in-situ damage sensors with usage monitoring in order to develop a structural health and integrity monitoring (SHIM) system for critical SOF components. The SHIM system could provide a continual assessment of the health and integrity of critical structural components that are not readily accessible. The in-situ damage sensors provide an inspection method with better access to difficult-to-inspect areas of complex structures while the flight data recorder provides parameters for computing actual structural loads for critical components. The application of a SHIM system in near real time would enable true condition-based maintenance in lieu of maintenance checks based on time of operation. Expected maintenance functions could be carried out only as need is established by the SHIM system. Further, flaw growth and structural failure could best be monitored by SHIM systems that continually, rather than periodically, assess structural health and integrity, thereby revolutionizing the approach to assessing the integrity of structures (Roach, 2007).

1.2 Technical Objective

The objective of this applied research project was to investigate the feasibility of integrating damage sensor

technology with current methodologies for usage monitoring and failure analysis into a SHIM system for military and civilian aircraft. The purpose of the SHIM system is to:

- (a) Assess the structural health and integrity of critical SOF components,
- (b) Reduce the likelihood of an in-flight break-up of aircraft due to structural failure, and
- (c) Increase maintenance effectiveness, thereby reducing downtime and increasing aircraft availability.

In order to meet the objective, the research focused on demonstrating the viability of integrating remote sensing for structural flaw nucleation and growth with intelligent reasoning logic and algorithms in order to discern the health and integrity of a complicated structural component under realistic loading. The research was performed on a critical SOF structure that is inaccessible and difficult to inspect using conventional NDI techniques. Researchers at Southwest Research Institute (SwRI) developed and integrated various technologies and methodologies that fused aircraft usage data, damage sensor data, and structural loads data with model-based and data-driven techniques for detecting incipient damage and assessing local/global structural health and integrity of critical SOF components.

1.3 Technical Approach

As illustrated in Figure 2, the development for a SHIM system involves the following process (Derriso, 2008).

- Identify the item of interest and its relevant failure modes
- Characterize the critical failure modes that result in system degradation
- Design a sensor system to capture degradation mechanisms
- Develop a component level reasoner to assess the current state of the component based on initial sensor output along with real-time and updated sensor output
- Predict remaining structural capability based on interpretation of sensor data and assumed operating conditions
- Output component assessment to a system level reasoner

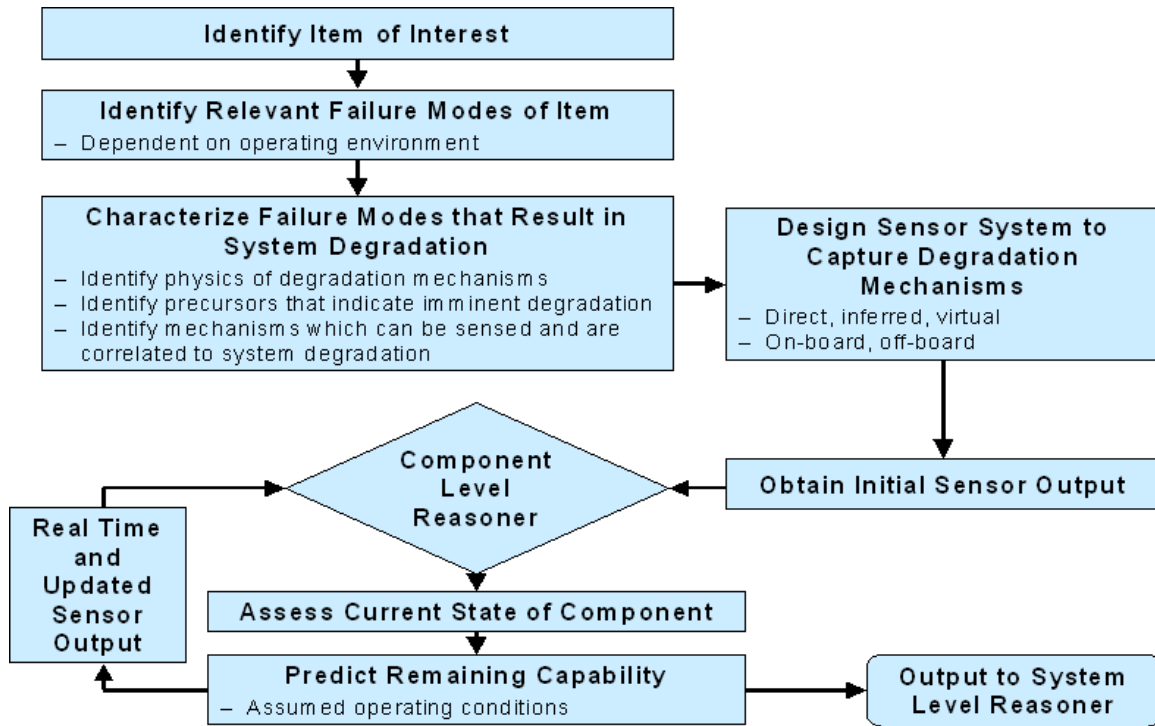


Figure 2: Development Process for a Structural Health and Integrity Monitoring (SHIM) System

For this research project, SwRI researchers drew on their extensive knowledge and expertise in aircraft usage, damage sensors, and structural loads data in order to apply the technical approach to a critical airframe SOF component. Figure 3 illustrates how the technical approach was applied to an actual airframe component, a fuselage longeron of a jet trainer aircraft. Previous structural life assessment and full-scale structural fatigue test provided detailed information on actual aircraft usage and structural loads data for this particular critical SOF component. During the full-scale test, the upper longeron was identified as a fatigue critical component, but conventional inspection techniques, such as a bolt hole eddy current inspection, require excessive maintenance man-hours and could potentially damage the structure during disassembly in order to access the splice. The emerging magnetostrictive sensor (MsS) technology, developed by SwRI, was incorporated into the design of a SHIM system for detecting, localizing, and assessing damage on a continual basis for the upper longeron. Demonstrating the feasibility of such a system on this component has applicability to similar critical components on many military and civilian aircraft, such as the wing spars and longerons that failed on the mishap aircraft discussed previously.

Following the SHIM development process, the internal R&D project involved the following primary tasks.

- Characterization of fatigue cracking, the primary failure mode in the upper longeron
- Design of a damage sensor system to capture degradation mechanisms
- Development of a component level reasoner to integrate damage sensor data with structural loads data and failure analyses in order to assess the current state of the component and predict the remaining capability
- Component testing of the system design in order to demonstrate the feasibility of the SHIM system
- Validation and assessment of the system design

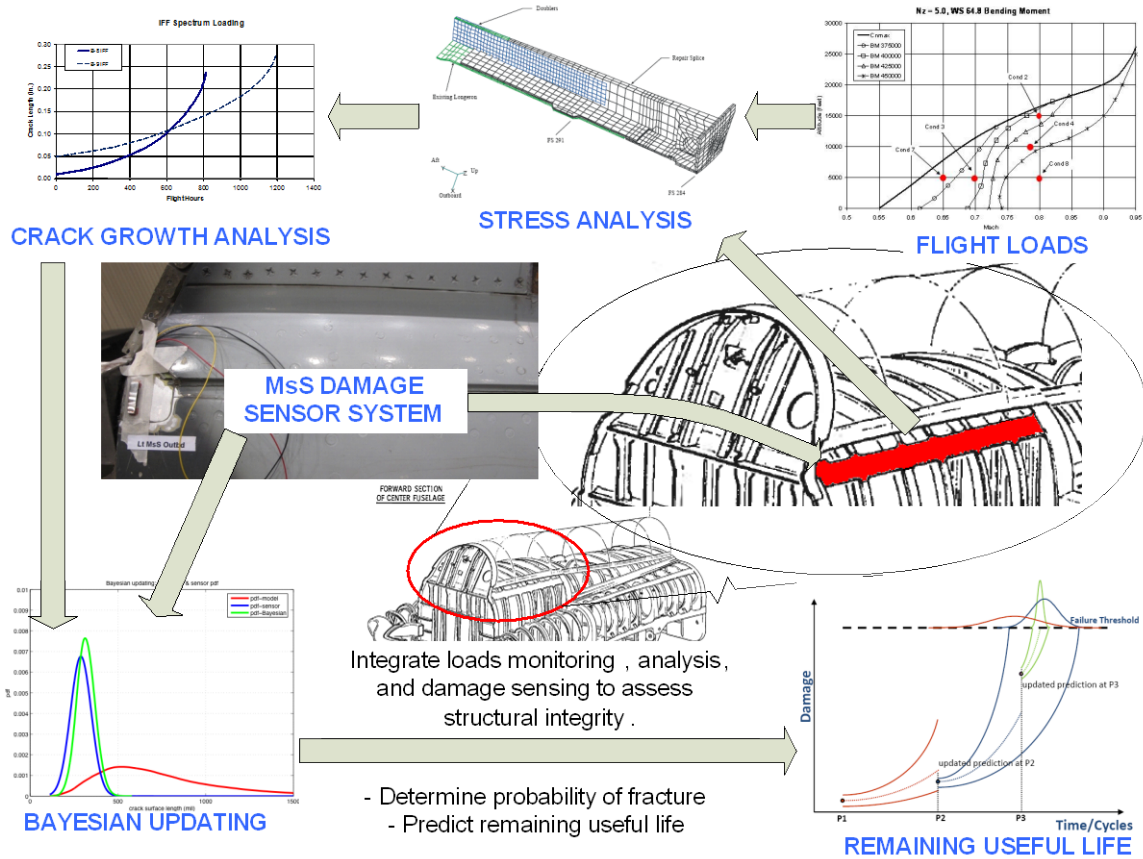


Figure 3: Technical Approach for Developing an Integrated Airframe Structural Health and Integrity Monitoring (SHIM) System

2. CHARACTERIZATION OF FATIGUE CRACKING (PROJECT TASK 1)

The upper longeron of a jet trainer aircraft is a primary structural component that transfers longitudinal loads along the fuselage between forward longerons along the cockpit and longerons along the aft fuselage. Due to stress corrosion cracking issues, a splice repair was installed on the upper longeron in order to replace a forward section of the longeron, as shown in Figure 4. Classical damage tolerance analyses and a structural system reliability analysis were performed on the upper longeron in order to identify critical locations, assess damage tolerance, and predict safety limits (i.e. critical crack length and residual strength) of the longeron, based upon damage severity and growth.

2.1 Damage Tolerance Analysis

Two fatigue critical locations (FCLs) have been identified on the upper longeron through damage tolerance analyses (DTA) (Wieland et al., 2009) and full-scale fatigue test of the fuselage (Burnside et al., 2007). One FCL is located on the flange of the

longeron splice, and the other FCL is located on the splice plates of the upper longeron. Based on the crack growth analyses, both of these locations have critical crack lengths of less than 0.30 inches, and under a severe flight load spectrum, their predicted crack growth lives to criticality are less than 1,200 flight hours. Using the Standard Practice under the Aircraft Structural Integrity Program (ASIP) (Department of Defense, 2005), initial inspections would be required at

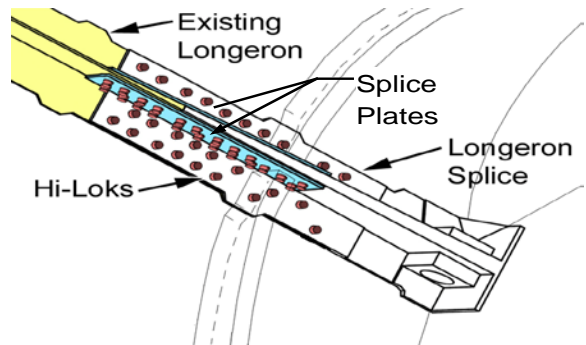


Figure 4: Splice Repair of Upper Longeron

less than 600 flight hours, with recurring inspections also occurring at less than every 600 flight hours. However, the inspection of these FCLs using conventional NDI techniques, such as bolt hole eddy current, would require excessive man-hours and could potentially damage the structure during disassembly in order to gain access to the FCLs in the splice.

2.2 Structural System Reliability Analysis

As part of a larger effort for investigating various analytical methods for use in structural health monitoring, a structural system reliability analysis was also performed on the upper longeron. This reliability analysis involved conducting a probabilistic risk assessment in order to determine critical locations of greatest concern in an airframe section that would benefit from a SHIM system. Two methods, Monte Carlo simulation (MCS) and another based on First Order Reliability Method (FORM), were used to perform a probabilistic risk assessment on all potential failure locations in order to identify the most likely failure locations in this complex structural joint (Smith et al., 2008 and Domyancic et al., 2009). Airframe components, such as longerons, are well suited for this investigation since they may likely have limited accessibility and be difficult to inspect using conventional techniques. As stated previously, DTAs and full-scale testing have shown that the splice joint in each longeron is fatigue critical. However, due to the complexity of the splice joint, it is difficult to determine which fatigue critical location in the joint could most likely cause a catastrophic failure.

Figure 5 shows the critical fastener locations identified through the probabilistic risk assessment on the actual longeron splice on the fatigue test article. This assessment confirmed the two FCLs (in the flanges of the longeron splice and in the splice plates)

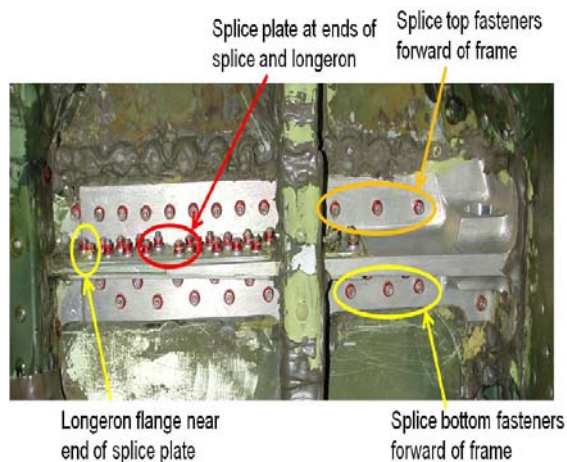


Figure 5: Critical Failure Locations on Upper Longeron

determined from the DTAs and full-scale fuselage fatigue tests. It also identified a third critical location in the existing longeron at the aft end of the splice plate, which was also identified in the full-scale fuselage fatigue test. A fracture mechanics model of this location was not available during the project in order to include it in the research. The structural system reliability analysis allowed researchers to determine specific locations in the joint where emerging sensor technology, such as the MsS technology developed by SwRI, could be incorporated into the design of a monitoring system for detecting, localizing, and assessing damage in the upper longeron.

3. DESIGN OF DAMAGE SENSOR SYSTEM (PROJECT TASK 2)

A damage sensor system, based on MsS technology, was designed for monitoring FCLs on the upper longeron. The MsS technology uses the physical property of a ferromagnetic material to generate an ultrasonic wave in a structure. This wave changes under mechanical stress (or strain), thereby providing the capability to capture damage, such as cracks, in a structure. Sensor locations that could detect, locate, and characterize damage at each FCL were identified on the upper longeron, and then, sensors were mounted on an actual airframe test article for component fatigue testing of the system design. Sensor data was collected and analyzed periodically during the fatigue testing in order to identify and track cracks developing and propagating during the test.

3.1 Basis for MsS Technology

The MsS technology is based on the Joule effect. When a ferromagnetic material is placed in a biasing magnetic field and then subjected to a time varying magnetic field, the magnetic domain in the material moves producing a mechanical wave. If the magnetic field is varied at a frequency greater than 20 kHz, the wave will be an ultrasonic wave. For wave detection, mechanical stress (or strain) causes a change in the magnetic induction of the ferromagnetic material, known as the Villari effect (Thwing et al, 2010).

Implementing the MsS technology involves adhesively bonding a thin (less than 0.010 inches) ferromagnetic strip to the surface of the structure and placing a MsS coil or probe over the ferromagnetic strip in order to excite the material. The excitation produces a guided wave in the material and generates waveform data for specific material and structural geometry (Thwing et al, 2010). The waveform data changes as damage propagates in a structure due to mechanical stress. By periodically monitoring the structure and collecting waveform data, this data can be compared to reference waveform data when no damage

existed in the structure. Monitoring data is generated by subtracting the individual waveform data from the reference data, thereby providing the capability to detect, locate, and characterize damage in the structure.

The MsS technology has excellent sensitivity to damage progression, such as crack propagation and corrosion growth, and it permits operation on any structural material. The sensors are very economical, making a system based on this technology ideal for long term monitoring of a large structure.

3.2 Placement of Sensors on Fatigue Test Article

Based on sensor testing conducted on salvaged upper longeron sections, MsS sensors were placed at several locations on a fatigue test article, which was a fuselage section that contained both the left hand (LH) and right hand (RH) upper longerons. Section 5 of this paper provides a detailed description of the test article and the component testing completed for the system design. The MsS sensor locations included four locations on each longeron. One sensor was mounted on the exterior surface of upper longeron and labeled "Lt/Rt MsS Outbd", as shown in Figure 6. This outboard sensor was used to monitor the longeron splice on the LH and RH upper longerons. Two more MsS sensor were placed inside the fuselage structure on the longeron splice just forward of the upper and lower splice plates in order to monitor the splice plates. Photographed in Figures 7 and 8, these sensors were labeled as "Lt/Rt MsS Top" or "Lt/Rt MsS Bot", based on their specific location and the longeron they were mounted on.

All of the MsS sensors used magnets strategically placed to achieve the desired bias field. This bias field produced an ultrasonic guided wave into the structure for monitoring the specific areas along the longeron splice and the splice plates. During the testing, a fatigue crack was discovered in the RH longeron flange near the aft end of the splice plates where no sensor had initially been positioned to monitor this location. Therefore, once these cracks were found, researchers mounted additional MsS sensors, labeled as "Lt/Rt MsS Aft", on the longeron flange several inches aft of the splice plates on both the LH and RH upper longerons in order to monitor any further crack growth at this location.

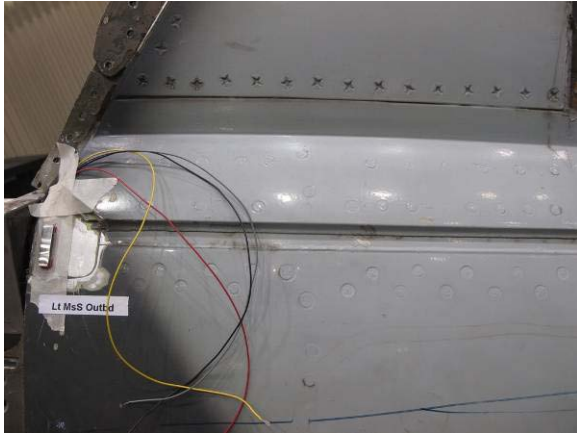
3.3 Sensor Data Collection and Results

Prior to the start of the fatigue test, sensor readings were collected at each of the MsS sensor locations to be used as a baseline for comparison to subsequent sensor readings collected at predetermined intervals of the fatigue testing. As described in detail in Section 5 of this paper, fatigue testing was conducted under spectrum cyclic loading for 12,500 simulated flight

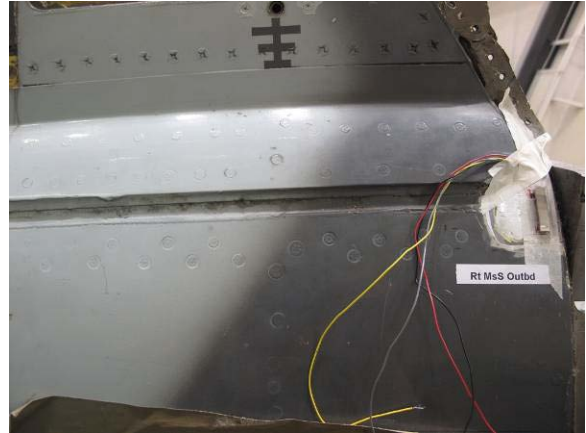
hours (SFH) with MsS sensor readings taken after every 225 simulated flights. Each MsS sensor reading was compared to the baseline reading at each location in order to determine if the sensor readings were increasing due to a crack indication or crack growth. No crack indications were identified by any of the sensor readings or any other monitoring method during the SFH cyclic testing.

In order to accelerate any crack growth and failure of a longeron, the fatigue testing was switched to constant amplitude testing. Another baseline MsS sensor reading was taken at each sensor location, and MsS sensor readings were collected every 2,000 cycles. During the constant amplitude testing, a crack nucleated in the RH longeron flange near the aft end of the splice plate, and the constant amplitude test was continued until the RH longeron severed due to fatigue loading. As previously stated, after this crack was identified, the MsS Aft sensor was mounted on both the LH and RH longeron flanges in order to monitor for continued crack growth. Because a baseline sensor reading had not been established for this location, the sensor readings from the LH longeron flange at this new MsS location were used as a baseline since the LH side had shown no indications of a crack at the time when the sensor was added. During the constant amplitude testing, cracks also nucleated and grew at the critical fastener locations on the upper and lower splice plates of the RH longeron. Twenty-five separate waveform data sets of MsS sensor readings were collected at each location during the constant amplitude testing with the exception of the two MsS Aft locations, which were added later, where fifteen data sets were collected.

MsS sensor readings from the constant amplitude testing were further analyzed after the completion of the test in order to determine if the sensors were able to identify any of the cracks observed during the test. Data from the Lt/Rt MsS Outbd sensors on both the LH and RH longerons were inconclusive, showing no increase in signal reflections. These results are expected since no fatigue cracks were identified in either the LH or RH longeron splices. Data collected from both the Lt MsS Bot and Rt MsS Bot sensors for the lower splice plates did not show any substantial change so these readings were not analyzed any further. Changes in the data sets could be seen in Lt MsS Top sensor for the upper splice plate indicating possible defect reflections, but the increase in signal reflection was not of sufficient magnitude to clearly indicate a defect.



a) Lt MsS Outbd

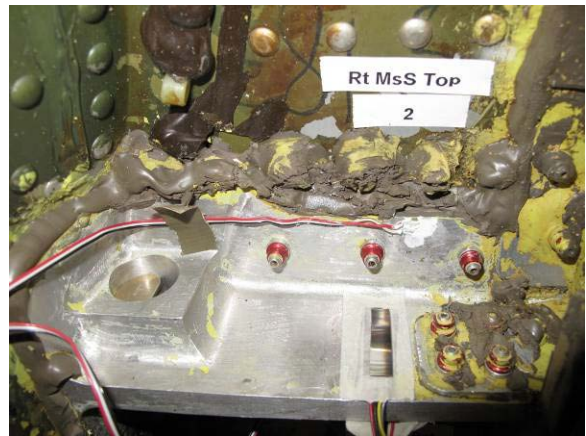


b) Rt MsS Outbd

Figure 6: Sensor Locations on Exterior Surface of Upper Longeron



a) Lt MsS Top

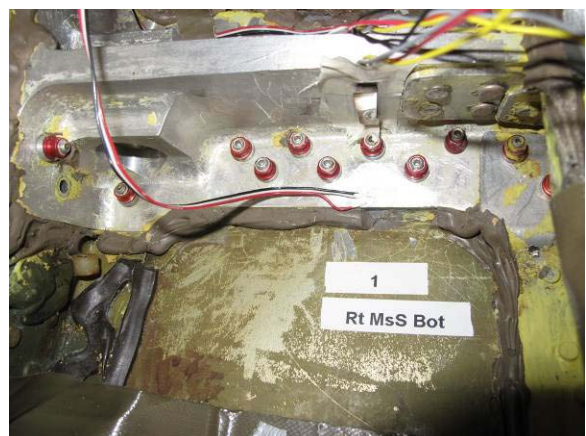


b) Rt MsS Top

Figure 7: Sensor Locations on Upper Splice Plates of Upper Longeron



a) Lt MsS Bot



b) Rt MsS Bot

Figure 8: Sensor Locations on Lower Splice Plates of Upper Longeron

Changes in the waveform data sets could be clearly seen in the Rt MsS Top sensor readings indicating defect reflections in the RH upper splice plates, as can be seen in Figure 9. Data collected from the Rt MsS Aft sensor also showed clear indications of crack growth in the RH longeron. Based on these sensor readings, the waveform data sets for the Rt MsS Top and Rt MsS Aft sensors were analyzed further in order to identify increases in sensor reflections that could potentially be correlated with any crack growth at these locations.

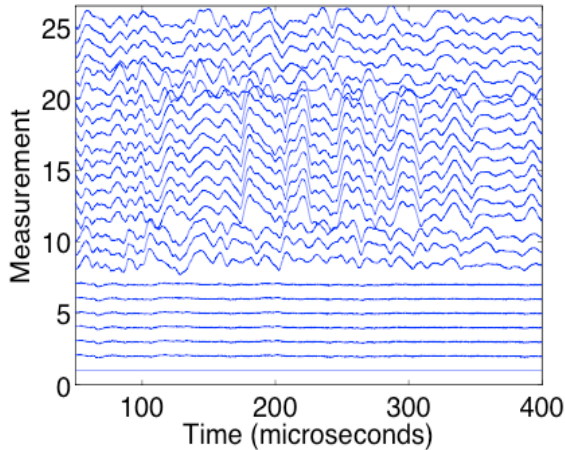


Figure 9: Waveform Data Sets from Rt MsS Top Sensor

Figure 9 shows a change on the seventh waveform data set for the Rt MsS Top sensor. The measurement number of the vertical axis denotes the sequential queries (or waveform data sets) of the MsS sensor readings taken as the fatigue test progressed. These data sets were analyzed further using SwRI developed Matlab software in order to focus in on the location where the defects may be located based on the sensor readings. Figure 10 shows data that was phase shifted to match the suspected defect location in time. Reflection differences were determined by comparing each sensor reading to the baseline reading at Measurement 0. Then, each of the reflections difference was stitched to make an energy plot of the wave forms representing an accumulated plot encompassing a 5- to 11-inch region along the longeron around the suspected defect. Figure 10 shows accumulated data stitched to create an energy plot of the data shown in Figure 9. The plot in Figure 10 represent a location in time that represents the possible reflected energy of a potential defect in the RH upper splice plate. The energy plot for the Rt MsS Top sensor does present a significant increase in the signal reflection, but these signals may also not be concrete evidence of crack detection and monitoring. Examination suggests that the noise associated with

each data set is attributed to a change in the magnetic bias field of each sensor itself and not of the specimen. This change may be due to possible shifting of the magnets that were attached to each sensor during large deflections of the structure due to the applied cyclic test loads.

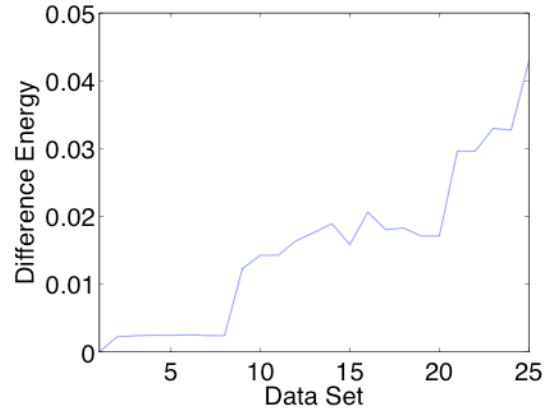


Figure 10: Energy Plot Rt MsS Top Sensor

Sensor readings collected from the Rt MsS Aft sensor are shown in Figure 11. Noting the horizontal axis is the distance from the probe and the signal fluctuations along this direction, clearly a reflection can be seen at approximately five inches from the sensor. This reflection slightly increases from one data set to another, and it is believed to be the signal from the crack in the RH longeron flange as the crack increases in size during testing. Figure 12 shows a close up view of the reflected energy window and the change in signal response from one query sample to another as data was accumulated. Figure 13 shows the energy responses for the area of interest in Figure 12 as the data was accumulated over time from the aft sensor. As expected, it shows a monotonically increase in energy amplitude from query to query.

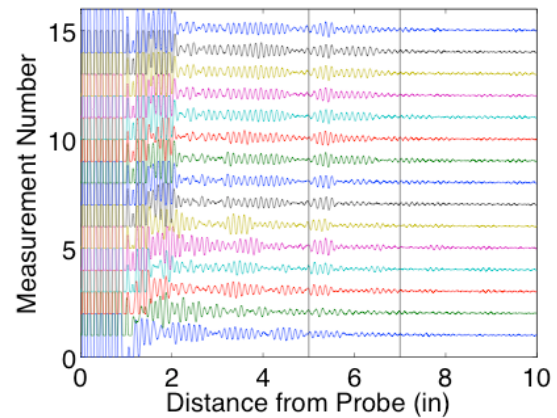


Figure 11: Waveform Data Sets from Rt MsS Aft Sensor

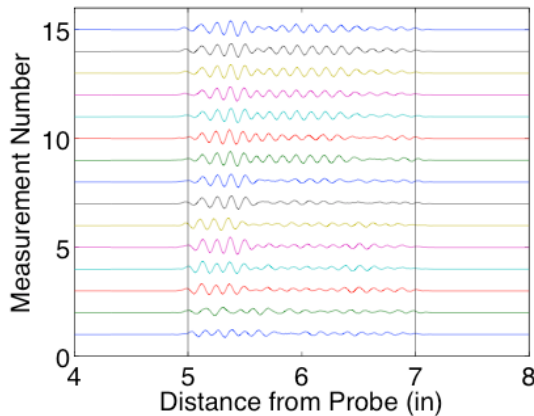


Figure 12: Close-up of Reflected Energy from Rt MsS Aft Sensor

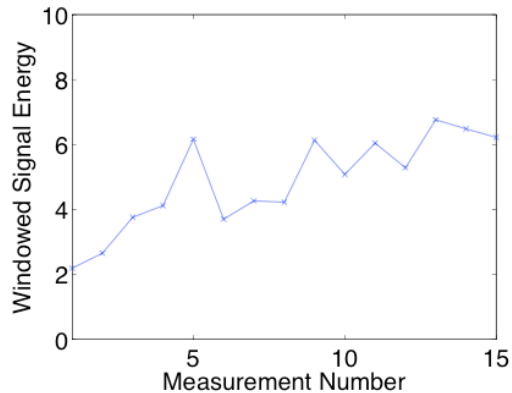


Figure 13: Energy Plot Rt MsS Aft Sensor

Based on these results, it was determined that monitoring with MsS sensors was feasible even though the bias fields of each sensor were not stable. The effectiveness of the MsS could likely be improved if stable bias fields could be maintained during monitoring. Additional research is also needed to further evaluate signal reflection for geometry changes during defect growth. Current MsS software needs additional modification in order to detect small changes associated with crack growth monitoring.

4. DEVELOPMENT OF INTELLIGENT REASONING LOGIC AND ALGORITHMS (PROJECT TASK 3)

Along with the DTA analyses of the critical locations, advanced monitoring strategies, and developed loading spectra for a critical structural component, a method was needed to integrate these independent pieces of the component's structural health picture into an assessment of the health and projected utility of the structural component. The following discussion on the

reasoning process outlines how this integration was accomplished in this research effort.

Researchers developed logic trees and intelligent reasoning algorithms that could be used to perform structural health and integrity assessments on critical airframe components. These logic trees and algorithms use existing software, analytical methodologies, and processes to perform the assessments based on operational flight data, crack growth analyses, and sensor data. As illustrated in Figure 14, the logic tree integrates usage monitoring with damage sensor data in order to assess the current health and integrity of the structural component.

The logic tree is composed of three main sections – one section for usage monitoring, another section for the damage sensor system, and the third section for integrating the analysis and sensor data with intelligent reasoning logic and algorithms for assessing the current state of the structural component. The usage monitoring section (left portion of the flowchart in Figure 14) includes algorithms for establishing flight regime, determining the stress spectrum for critical locations based on actual flight loads, and performing crack growth analyses of critical locations under actual usage. In the reasoning process, this usage monitoring provides the analyst with the predicted state that flaws in the critical areas should be in based on the measured or actual flight usage.

In the section for the damage sensor system (right portion of the flowchart in Figure 14), Boolean logic is used to determine if a flaw is detected, and if so, a flaw size distribution is estimated based on correlation of signal amplitude to damage size at critical locations. As discussed in Section 6 of this paper, this correlation was determined from fatigue testing of the structural component with a prototype MsS damage sensor system used to monitor the component during the testing. The damage sensor system provides the most likely state of flaws in the critical areas, which the analyst uses with the predicted state of flaws in the reasoning process in order to assess the component's health and integrity.

The assessment section (box illustrated in the lower right corner of Figure 14) integrates the analysis and sensor data to estimate the flaw size distribution in the component. Then, based on this estimated flaw size distribution and assumed future operating conditions, the remaining useful life and likelihood of structural failure are computed for the structural component. The reasoning process for the structural health and integrity assessment is described in the following paragraphs.

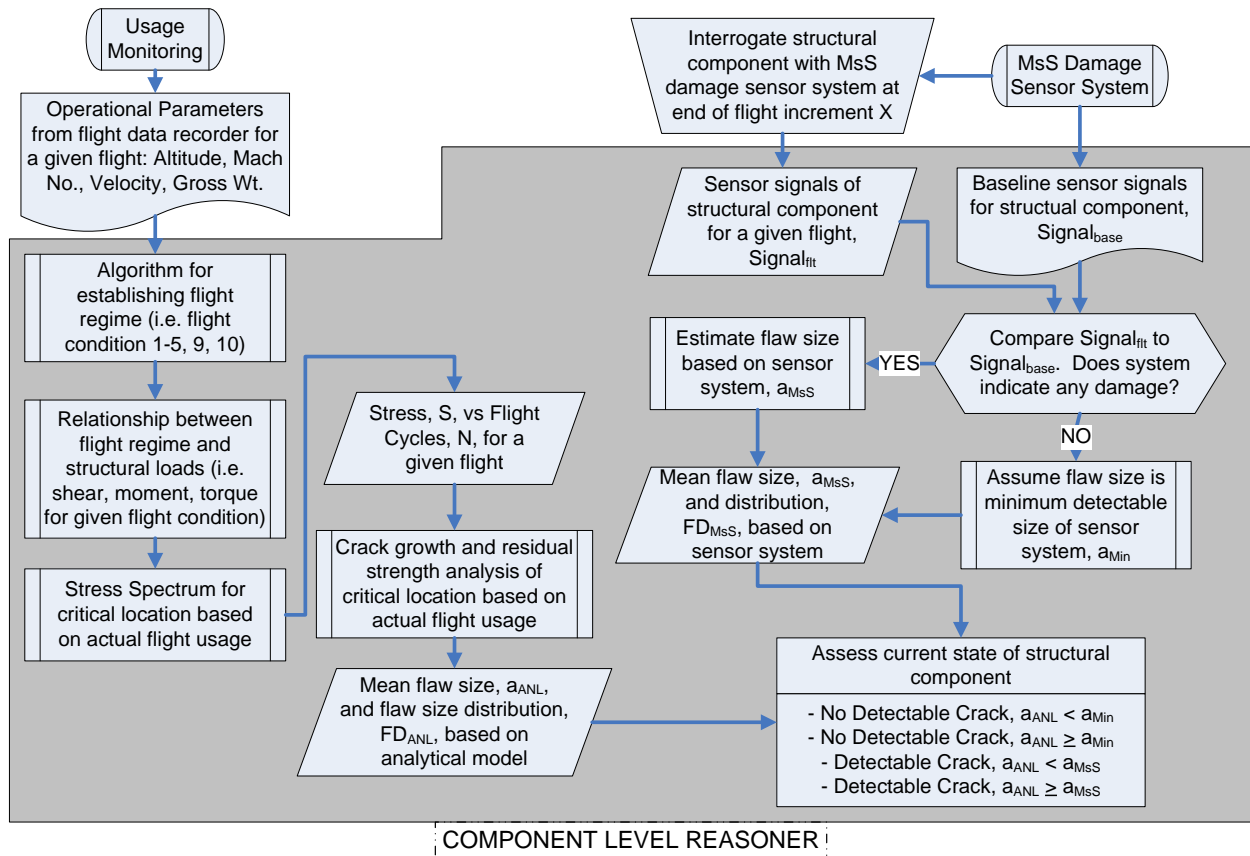


Figure 14: Logic Tree for Component Level Reasoner

4.1 Usage Monitoring

Algorithms are already used as part of the aircraft’s Individual Airplane Tracking Program (IATP) to define the stress spectrum from the actual operational flight parameters for particular FCLs. These same algorithms were used in order to conduct crack growth analyses for the two FCLs on the upper longeron based on actual usage monitoring. These algorithms involve the following four step process.

1. Identify significant peaks and valley vertical acceleration (Nz) events using 0.5g delta criteria.
2. For each significant Nz event, identify the representative flight condition based on the flight parameters Nz, Altitude, and Mach Number.
3. For the given flight condition and associated gross weight, compute the structural loads at the critical component.
4. Compute event stress using the defined stress-to-load ratio for the given FCL and the defined gross weight ratio.

Once event stresses were computed and a stress spectrum defined for each flight, crack growth analyses were conducted for each FCL by employing conventional linear elastic fracture mechanics (LEFM) methods. These crack growth analyses established a distribution of flaw sizes (FSD_{ANL}) with an analytical mean flaw size (a_{ANL}) at pre-defined flight intervals for both the longeron splice and splice plates based on LEFM models and predicted flight loads.

4.2 Structural Damage Sensing

For the MsS damage sensor system, the following process was employed for collecting sensor data and monitoring the structural component on a continual basis.

- Sensor readings were collected on the critical structural component prior to application of flight or cyclic loads in order to establish a baseline for comparison to subsequent readings.
- At a predetermined flight or cycle increment (given as a measurement number as referenced previously), the structural component was interrogated with the MsS sensor system, and

readings were collected for each sensor location on the component.

- The sensor signal at the predetermined flight or cycle increment was compared to the baseline signal for each location of interest in the structure.
- Based on changes in the recorded signals from baseline to the current measurement, boolean logic was used to determine if a flaw was detected (i.e. Was signal amplitude > detectable level?). Flaw detection and size was based on the previous correlation test that used known induced flaw sizes to calibrate the difference between signal amplitude and damage size at the FCL. This correlation was refined based on signal amplitudes measured during the fatigue test and flaw sizes observed at the FCL during the teardown examination.
- If the sensor signal did not indicate a flaw, the flaw size was assumed to be at the minimum detectable level.
- If the sensor signal did indicate a flaw, the flaw size was estimated based on the signal amplitude and the previous correlation to damage size.
- Depending on the sensor amplitude, a mean inspection flaw size (a_{MsS}) and flaw size distribution (FSD_{MsS}) was estimated based on the readings from the MsS damage sensor system.

4.3 Reasoning Logic and Algorithms for Structural Health and Integrity Assessment

Reasoning logic and algorithms were developed to perform a structural health and integrity assessment of a critical structural component based on sensor data, simulated flight load data, and crack growth analyses. The algorithms use Bayesian principles to fuse sensor signals with crack growth analyses in order to estimate a mean flaw size (a_{SHM}) and its distribution (FSD_{SHM}) based on the SHIM system. Illustrated in Figure 15, the reasoning logic computes a remaining useful life and conditional failure rate based on interpretation of the sensor and analytical data along with assumed future operating conditions.

The component-level reasoning process described in Figure 14 consists of two separate methods of estimating the size of a crack/flaw – one method based on actual usage and crack growth analyses, another method based on sensor signals and correlation of signal amplitude to known flaw size. To rectify the differences in these estimates, which are certain to exist, probabilistic methods can be applied. Before going into detail on the methods, it is important to point out that these methods, while powerful, are predicated on the ability to accurately assess uncertainty of the individual estimating processes. Poor uncertainty estimates for either method will tend to lead to non-optimal combined estimates and may ultimately lead to misleading results. In particular, overestimating the accuracy of either estimate may bias the combined results strongly toward that estimate.

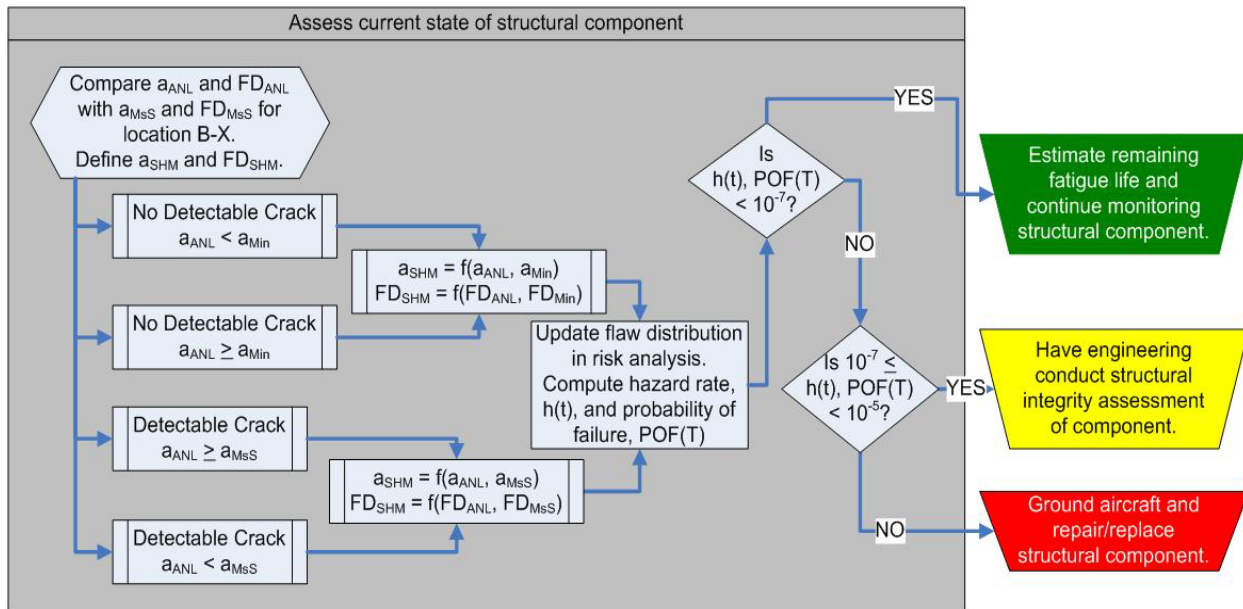


Figure 15: Reasoning Logic Tree for Structural Health and Integrity Assessment

A Bayesian estimation process can be used to rectify sensor readings with analytical predictions of crack size. Given the recurring nature of the sensor readings, herein referred to as measurement, and prediction processes, a recursive Bayesian estimation process is appropriate. A Kalman filter is a well-known and powerful type of recursive Bayesian estimator. A standard Kalman filter assumes that the system that is being predicted is linear and that the probability distributions are all Gaussian. Unfortunately, the crack growth model that is used for prediction is nonlinear, and the prior probability distribution for initial flaw size is distinctly non-Gaussian. Although approximations can be made from which to make use of the Kalman filtering approach, the generalized Bayesian estimation process is relatively straight-forward for this type of problem, so accuracy does not need to be traded for convenience.

The single-degree-of-freedom continuous probability distribution form of Bayes' law is given by:

$$f_C(c|z^*) = \frac{f_Z(z^*|c)f_C(c)}{f_Z(z^*)} \quad (1)$$

where f is the marginal probability density function (PDF) with respect to the subscripted variable. Here c is a random variable representing the crack size, while z^* is the value of a measurement of the crack size. This formula can be interpreted as: the probability of a crack size c given a measurement of z^* is equal to the probability of the measurement z^* given a crack size of c times the *a priori* probability of a crack size c divided by the prior probability of a measurement of z^* . Putting the estimate in this form is useful because the marginal density function $f_C(c|z^*)$, which is the distribution of interest, cannot be evaluated directly, but the terms on the right-hand side of the equation can. The prior probability term $f_C(c)$ is the probability of a crack of size c existing at the point of interest on the structure. For the reasoning algorithm, this prior probability is estimated using the crack growth model starting from an initial flaw size distribution. The prior probability of measurement $f_Z(z^*)$ is calculable but non-essential in this equation because it is simply a constant – z^* is a single value of a measurement of the crack size and does not affect the shape of the distribution. Finally, the marginal density of measurement z^* given crack size c , $f_Z(z^*|c)$, is

simply the uncertainty (or error distribution) of the measurement.

If only a single attempt is made to estimate the size of a crack, this form is sufficient, but the reasoning algorithm is meant to be applied repeatedly over the life of the structure. In the case of recurring estimates, we would like to refine the prior probability distribution to account for the estimates that have been made up to the current time. For the recursive case, Bayes' law is written as

$$\begin{aligned} f_C(c_k|Z_k) &= \frac{f_Z(z_k|c_k)f_C(c_k|Z_{k-1})}{f_Z(z_k|Z_{k-1})} \\ &= \alpha f_Z(z_k|c_k)f_C(c_k|Z_{k-1}) \end{aligned} \quad (2)$$

In this case, the prior probability density for the crack size is given by $f_C(c_k|Z_{k-1})$, providing the recursive element to the equation. Z_k represents the measurements from all k iterations of the estimation process. So the current estimate (the k^{th} iteration) is based on the predicted crack size estimate based on the $(k-1)^{\text{th}}$ estimate combined with the current measurement $f_Z(z_k|c_k)$. Note that $f_Z(z_k|Z_{k-1})$ is just a constant. Written in a slightly more accessible form, the estimation process can be described by:

$$f_{est}(k) = \alpha f_{meas}(k) f_{pred}(f_{est}(k-1)) \quad (3)$$

Here, the k^{th} estimate is the product of the current measurement distribution $f_{meas}(k)$ and the distribution that is predicted from a crack growth model, $f_{pred}(f_{est}(k-1))$, using the prior iteration's estimate for crack size as the initial condition, while α is a normalization term that ensures that $\int_C f_{est}(k) = 1$.

For Gaussian distributions, this estimation process is equivalent to weighted averaging based on the variance of the distributions. The resulting Bayesian estimate would have a mean of

$$\mu_{est} = \frac{\sigma_{meas}^2 \mu_{pred} + \sigma_{pred}^2 \mu_{meas}}{\sigma_{pred}^2 + \sigma_{meas}^2} \quad (4)$$

and a variance of

$$\sigma_{est}^2 = \frac{\sigma_{pred}^2 \sigma_{meas}^2}{\sigma_{pred}^2 + \sigma_{meas}^2} \quad (5)$$

For example, suppose the predicted crack size distribution has a mean of 0.35-inch and a standard deviation of 0.05-inch, while the measurement distribution has a mean of 0.45-inch and a standard deviation of 0.03-inch. Figure 16 shows these distributions along with the resulting Bayesian estimated crack length distribution, which illustrates how the estimate has a higher certainty than either the prediction or the measurement alone.

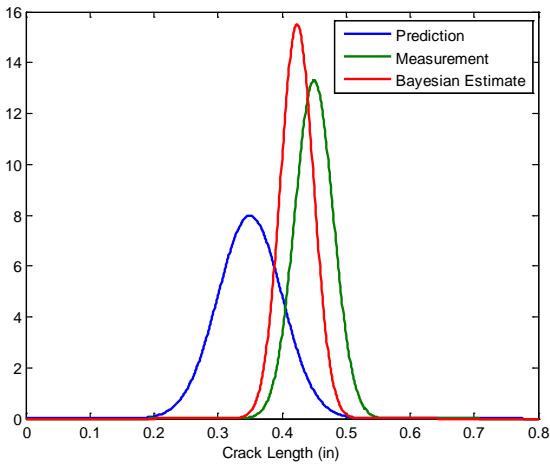


Figure 16: Iteration Example of Bayesian Estimation Process for Gaussian Distributions

For non-Gaussian distributions, which are more typical for this type of application, the underlying process is the same, but computation of the resultant distributions must typically be done numerically. Figure 17 provides an example of the estimation applied to a prediction that is non-Gaussian and a measurement that is Gaussian. The resultant distribution is non-Gaussian.

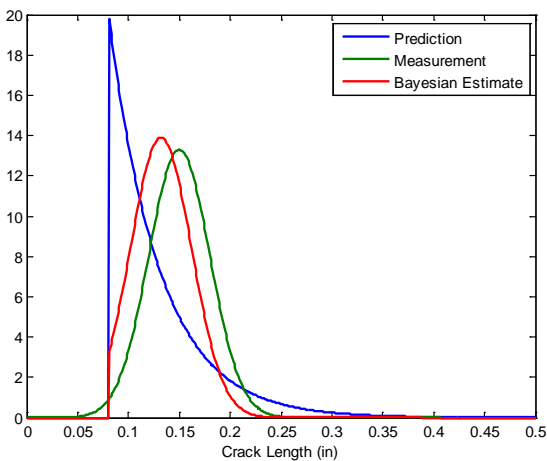


Figure 17: Iteration Example of Bayesian Estimation Process with a Non-Gaussian Distribution

Although Bayesian estimation is robust to uncertainty in the constituent estimates, several caveats must be noted. First, all constituent estimates, specifically their probability distributions, must be defined over the same domain. This may seem obvious, but when dealing with arbitrary numerical distributions, absence of data or lack of detail, particularly in the tails of the distributions, can lead to a final estimate with a distorted distribution. Second, even though a mathematically optimal estimate can be obtained for any set of constituent distributions, it is important to ensure that differences between the constituent estimates do not stem from issues not accounted for in the probability distributions (an inoperable sensor, for instance). For example, suppose we use two different sensors to measure the size of a crack. Furthermore, let us assume that both sensors are similar in performance such that their measurements will yield values that are within ± 0.025 -inch of the actual crack length with 95% confidence. Now assume that during one measurement of a crack, one sensor reports a crack length of 0.200-inch while the other reports 0.400-inch. Given that information, it is possible to compute an optimal estimate of 0.300-inch, but the more likely reality is that one or both of the sensors is reporting an incorrect measurement. The optimal value is well into the outlier range (in this case about eight standard deviations out) with respect to both constituent measurements. Large normalization terms, α , for the Bayesian estimated distribution tend to indicate poor agreement between constituent distributions.

4.4 Assessment of Structural Health and Integrity

For assessing the structural health and integrity of the upper longeron, analytical prediction distributions were generated by starting with an initial flaw size distribution (obtained from the literature) and running crack growth simulations for points along the distribution. Because the crack growth model preserves the relative ordering of the crack lengths (i.e. a small crack will not out-grow a larger crack in the same location, under the same loads, etc.), the predicted distribution can be calculated directly from the initial distribution, without the need for an intermediate random sampling process. The resulting crack lengths predicted using the crack growth model are just associated back to probability density associated with the initial crack lengths. In this manner, the shape of the distribution is shifted, but the relative probability distance between the crack lengths that make up the distribution stays the same.

Then, Bayesian principles are used to fuse the estimated flaw size from sensor signals with flaw size predictions from crack growth analyses (Hudak et al.,

2007). Figure 18 shows an example of how Bayesian principles are used to integrate sensor signals with crack growth analyses for the upper longeron. At given number of operational flight hours, the analytical crack growth model provides a cumulative density function (CDF) of the flaw size based on actual usage. Data from the damage sensor system also provides a CDF based on the signal amplitude of the sensor. Using Bayesian principles, these two CDF's are updated into one CDF estimating the flaw size distribution. This final estimate is based on a weighted average of both the analysis and sensor information. In this example, the flaw is below the minimum detectable level of the sensor so for the Sensor CDF, it is assumed that the flaw size is at the minimum detectable level of 0.045-inch with a wide range in the flaw size distribution (variance of 0.0004-inch^2). Initially, with a fewer number of flight hours, the crack growth analysis predicts a relatively small flaw size distribution so the Average CDF favors the Analysis CDF. As the flight hours increase, the Analysis CDF increases, and eventually, the crack growth analysis predicts possible fatigue failure of the component. However, the Sensor CDF remains the same since the sensor has not detected a flaw. Therefore, the Average CDF favors the Sensor CDF. Utilizing the Average CDF to estimate the flaw size allows for a more accurate prediction of the

remaining useful life and likelihood of structural failure, as described in the following paragraph.

Updated flaw size distributions can be used to compute conditional failure rates and remaining useful life, as illustrated in Figure 19. The distribution of results for each of the three stages of measurements is plotted at the top of the graph at the damage level defined as the failure threshold. These distribution plots illustrate how the predictions tighten up as more information is measured. Initially (point P1), analysis predicts sufficient remaining useful life with a low probability of structural failure, but the life prediction varies widely. As the life prediction is updated with the Average CDF (point P2), the range in life prediction tightens, and the likelihood of structural failure increases. As the component reaches the end of its useful life (point P3), the range in life prediction narrows, and the likelihood of structural failure reaches unacceptable levels. Each update is based on a weighted average of the flaw size distribution from the sensor data and crack growth analyses, instead of solely relying on either the sensor or the analyses. Using the weighted average CDF provides an improved estimate of the remaining useful life and probability of structural failure.

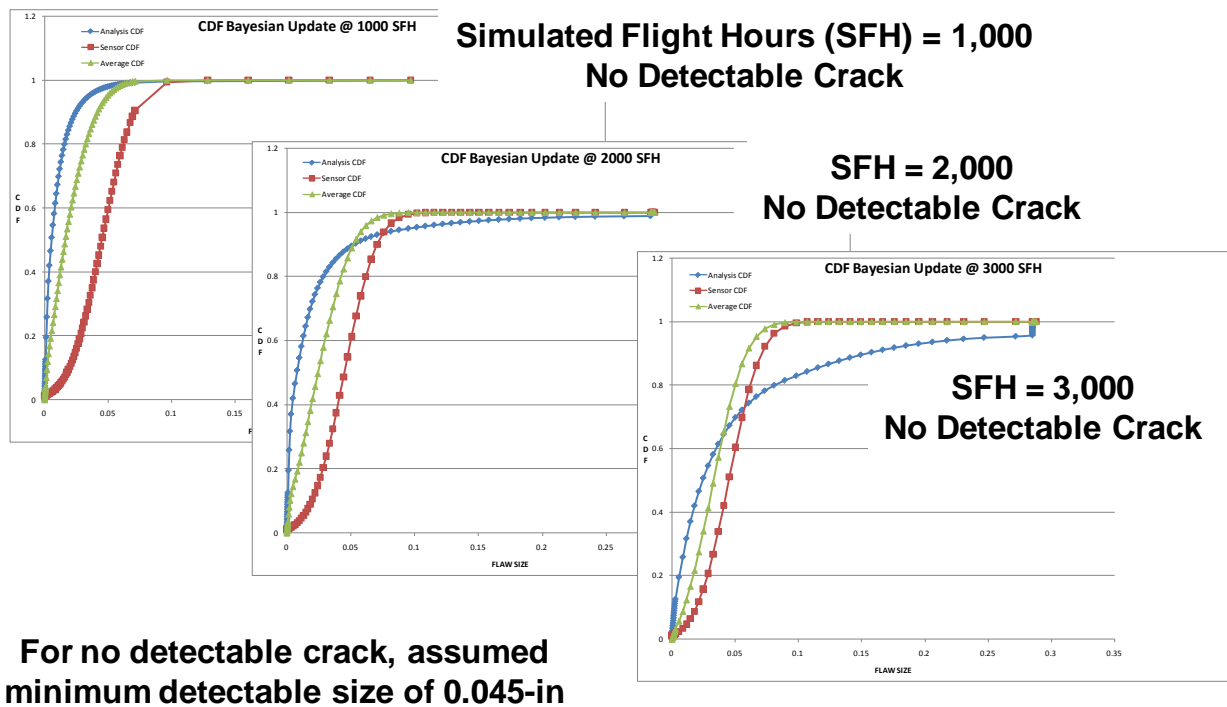


Figure 18: Fusing Sensor Signals and Analytical Crack Growth Using Bayesian Updating

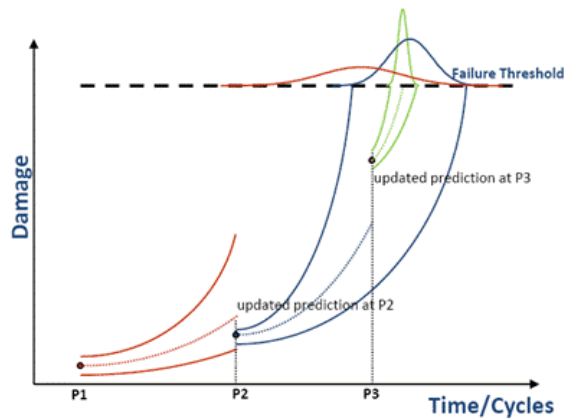


Figure 19: Prediction of Remaining Useful Life Based on Updated Flaw Size Distribution

The Bayesian updating is used to predict the remaining useful life and probability of structural failure for the upper longeron as it was being subjected to cyclic loading during a fatigue test, which is described in detail in Section 5 of this paper. Applied stresses, based on strain gauge readings at critical locations, were recorded during the cyclic testing, and readings from the MsS damage sensor system were collected at predetermined flight intervals for each of the monitoring locations on the test article. Crack growth analyses were performed using the actual applied stresses in order to provide an analytical prediction of crack growth life, and sensor readings were used to estimate the actual flaw size at the critical locations.

Figure 20 shows the crack growth life predictions for the splice plates of the upper longeron utilizing three different methods. The first method is the conventional DTA methodology described in Section 2.1, which starts with a rogue flaw of 0.05-inch and has a fatigue life of only 1,215 simulated flight hours (SFHs). The second life prediction starts with an initial flaw size distribution for 7075-T6 plate (obtained from the literature) that has a mean flaw size of 0.0061-inch. With this initial flaw size, the fatigue life prediction is 5,174 SFHs based on LEFM and the actual spectrum loads applied during the fatigue test. The third life prediction method employs Bayesian updating to estimate the flaw size periodically during the fatigue test based on the crack growth analyses and readings from the MsS damage sensor system. During the fatigue test, spectrum flight loads were applied for 12,500 SFHs, and sensor readings were taken approximately every 250 SFHs. No crack indications were ever identified by the sensors during the SFH fatigue testing. Subsequent teardown examination confirmed that the upper longerons did not have detectable cracks during the simulated flight spectrum testing. Since the sensors did not detect any cracks, it

was assumed that any cracks in the splice plates was at the sensor's minimum detectable level of 0.045-inch, and flaw size distributions were updated accordingly at the time frame for each sensor reading. Utilizing the Bayesian updating, the averaged flaw size stayed below the minimum detectable level for the entire spectrum fatigue testing, as indicated by the green triangular assessment points plotted in Figure 20. Even though initially the averaged flaw size was larger than the analytical flaw size, the averaged flaw size never exceeded the minimum detectable level of the sensor, and the crack growth life predictions, which were updated at each interval of sensor readings, never reached critical crack length. Both of these conditions were confirmed through the fatigue testing and teardown examination.

Probability of failure (POF) analyses were also performed at each interval of sensor reading using the averaged flaw size and its distribution, which was continually updated based on Bayesian principles. Figure 21 compares the POF results based solely on LEFM crack growth predictions to POF results utilizing the SHIM system. These analysis results clearly show that continual monitoring and updating the estimated flaw size with its distribution can reduce the POF by at least an order of magnitude, with the exception of one interval of 500 SFHs where the POF utilizing the SHIM system was the same as the POF based solely on analytical predictions. When the averaged flaw size reached a constant value of 0.0375-inch, just below the minimum detectable level for the sensor, the POF analyses based on the SHIM system leveled off, never increasing by more than three orders of magnitude during the monitoring interval of 250 SFHs. Using the same reasoning processes in the SHIM system, the POF could likely be reduced even further if the monitoring interval had been shortened. The analysis results in Figures 20 and 21 illustrate how predictions of remaining useful life and probability of failure assessments can be improved with continual structural health monitoring.

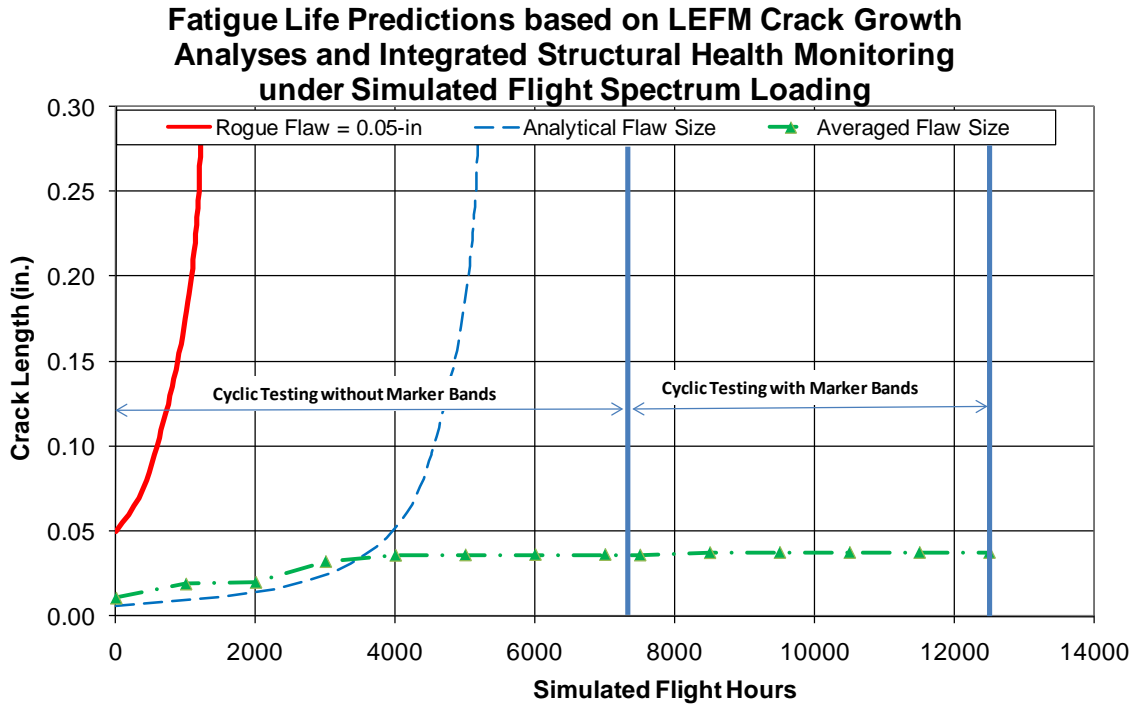


Figure 20: Fatigue Life Prediction of Upper Longeron Splice Plates

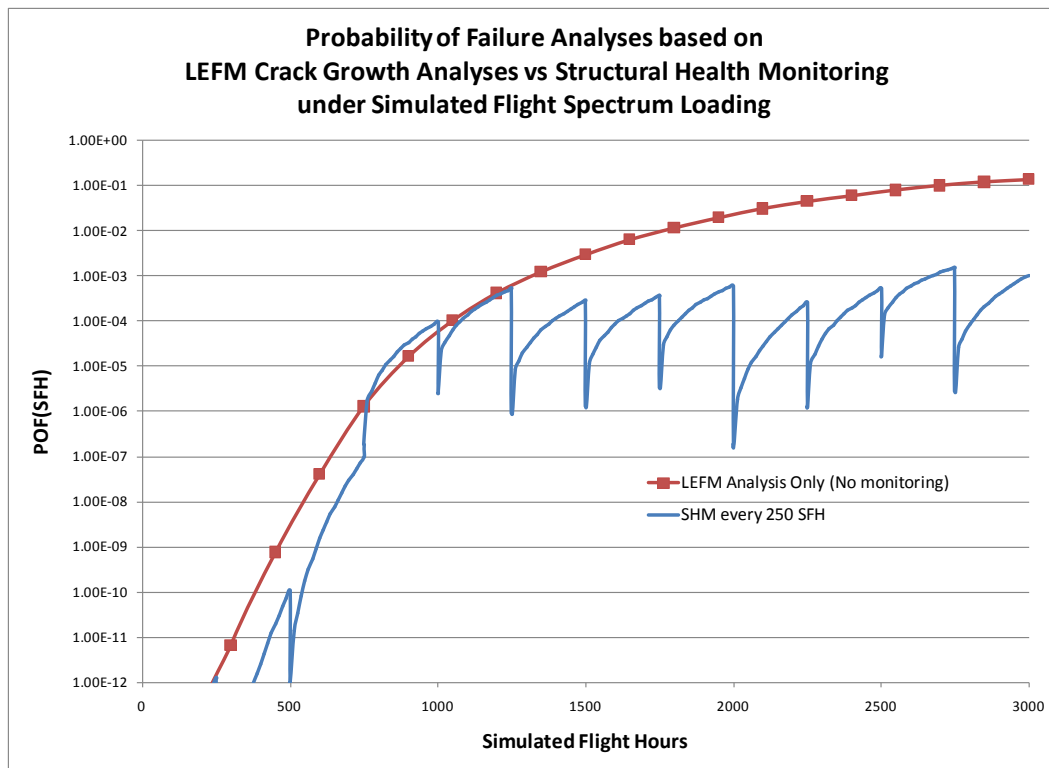


Figure 21: Probability of Failure Analyses of Upper Longeron Splice Plates

5. COMPONENT TEST OF SYSTEM DESIGN (PROJECT TASK 4)

In order to demonstrate the feasibility of using an SHIM system on an actual critical structural component of an aircraft, researchers and structural test engineers designed and conducted a fatigue test of a fuselage section containing the LH and RH upper longerons. Extracted from a condemned fuselage, this airframe section was instrumented with the MsS damage sensor system to monitor critical locations and with strain gauges to monitor actual loads being applied across the upper longerons. Damage sensor readings and crack growth analyses based on the loads monitoring were interfaced with the intelligent reasoning logic and algorithms in order to continually assess the structural health and integrity of the upper longerons during testing. After setting up the fatigue test and instrumenting the test article, the component test was conducted under both spectrum flight loads and constant amplitude loads.

5.1 Test Setup

After extracting the airframe section from a condemned fuselage, technicians modified the test article and constructed a test fixture so that each upper longeron could be loaded in tension using a single load actuator. Strain gauges were installed on the test article at various locations across the upper longeron splice along with MsS sensors. As illustrated in Figure 22, strain gauges were installed on the lower and upper flanges of the longeron splice (SG1/SG2 on the RH longeron splice, SG7/SG8 on the LH longeron splice). Strain gauges were also installed on the lower and upper splice plates (SG3/SG4 on the RH splice plates, SG9/SG10 on the LH splice plates). Additional strain gauges were placed on the upper and lower flanges of the original longeron just aft of the splice plates (SG5/SG6 on the RH longeron, SG11/12 on the LH longeron). A data acquisition system was built and programmed for collecting sensor and strain gauge data during the fatigue test. A load controller was also programmed, calibrated, and tested to insure that correct load levels were introduced into the fuselage article during fatigue testing. Figure 23 is a photograph of the test article mounted in the fixture, the MsS damage sensor acquisition unit, and the data acquisition hardware (shown from right to left).

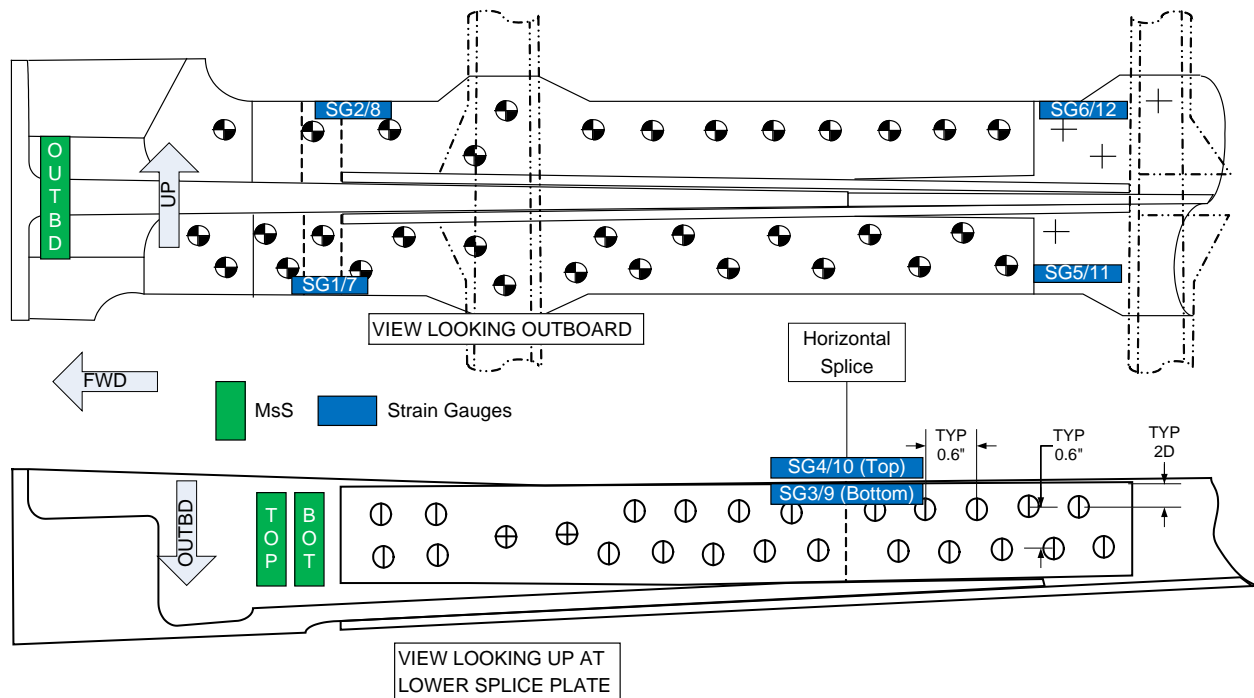


Figure 22: Strain Gauge and Sensor Locations on Longeron Splice

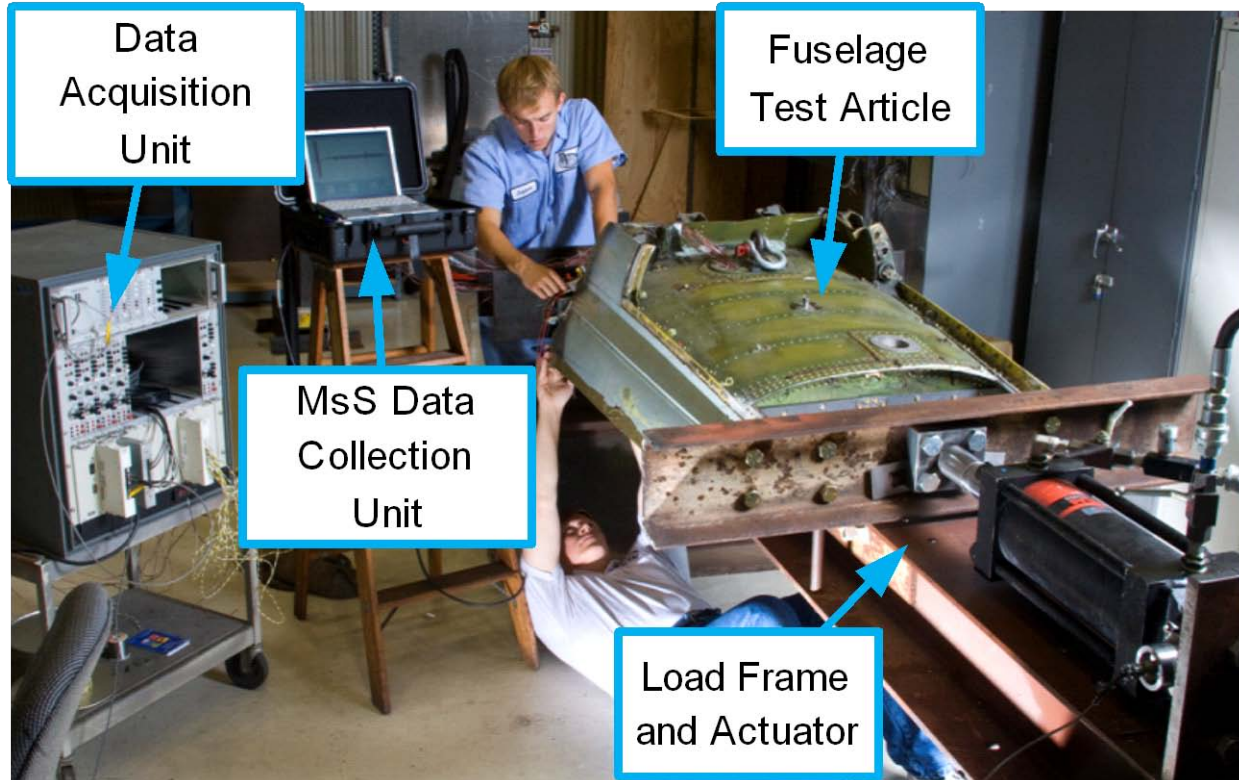


Figure 23: Fatigue Test Setup of Upper Fuselage Section

5.2 Methods for Structural Health and Integrity Monitoring

Three different methods were used during the fatigue test to monitor the structural health and integrity of the upper longeron splice.

- The primary monitoring method was periodic ultrasonic scans with the MsS damage sensor system. At specified intervals during the fatigue test, signal data was collected from the three MsS sensors mounted on the both the LH and RH upper longeron splices.
- As a secondary method, structural loads monitoring was used to monitor stress levels in the upper longerons. Stress values were recorded at each strain gauge for pre-determined applied load levels from the fatigue test spectrum. Trends in stress values inferred from the strain gage readings were monitored during the fatigue test in order to determine when and where load started increasing or decreasing significantly over normal stress levels in the structural component.
- For the third monitoring method, researchers used a conventional nondestructive inspection technique to perform periodic surface eddy current scans around all fasteners in the upper longeron.

5.3 Fatigue Testing using Simulated Flight Hour and Constant Amplitude Spectrum

Three different test spectrums were used for the fatigue test. Initially, the test was conducted with a cyclic load spectrum that simulated severe flight conditions for the upper fuselage and with no flaws induced in the test article. The test was run for 7,500 SFHs with this severe spectrum, and no damage was observed in the test article with any of the monitoring methods during this first set of flight spectrum testing. In order to accelerate the fatigue test, 0.05-inch corner flaws were induced at three fastener locations on each longeron – one in the lower flange of the longeron splice and one each in the critical fastener locations on the upper and lower splice plates. Then, marker band load cycles were added to the severe load spectrum in order to assist with tracking crack growth during the post-test teardown examination. The test was run for another 5,000 SFHs with the severe spectrum and marker bands. Again, no damage was observed in the test article with any of the monitoring methods. Therefore, the load spectrum was switched to a constant amplitude spectrum in order to rapidly accelerate the fatigue test and induce fatigue failure of the test article while using the various monitoring methods.

After 12,500 SFHs of flight spectrum testing, the load spectrum was switched to a constant amplitude spectrum at a high operational load level so that researchers could quickly create fatigue damage in the test article and cause catastrophic failure of the test article. Illustrated in Figure 29, the constant amplitude spectrum consisted of 2,000 cycles at a pre-defined load level, of either 12-ksi or 15-ksi, followed by a series of marker band cycles in order to assist with tracking crack growth during the teardown examination. MsS sensor readings were taken at each sensor location at the end of each marker band cycle block. As discussed below, the constant amplitude fatigue testing resulted in several fatigue cracks developing in the splice plates on both the LH and RH longerons. The constant amplitude fatigue testing also resulted in a crack nucleating in the flange of the RH original longeron, which led to this longeron being severed due to fatigue damage.

5.4 Loads Monitoring During Fatigue Test

The structural loads monitoring performed during the fatigue test provided an excellent means for identifying where damage was occurring in the structure. Figures 24 and 25 shows the trends in the loads monitoring observed during the constant amplitude fatigue testing. Initially, the fatigue test was conducted at a constant

amplitude command load level of 12-ksi for 16,340 cycles. Then, the load level was increased to 15-ksi, and during the loads monitoring, researchers noticed stress levels dropping off dramatically in the upper splice plate on the RH upper longeron (Fig. 24, SG4) while the stress level increased on the lower splice plate (Fig. 24, SG3). During these changes in stress levels, a crack was found visually in the flange of the RH upper longeron at the aft end of the splice plates. The crack was located at the fourth critical location identified in Project Task 1, but not initially monitored with MsS sensors. At 32,680 cycles, surface eddy current scans identified cracks in both the upper and lower splice plates on the RH upper longeron. As the fatigue test continued, stress levels increased in the RH upper longeron itself just aft of the splice plates (Fig 25, SG5/6) while the stress levels continued to drop off in the upper and lower splice plates on the RH upper longeron (Fig 24, SG3/4). Eventually, the stress levels in the RH upper longeron (Fig. 25, SG5/6) dropped off dramatically, and the RH upper longeron severed at 54,542 cycles. The test article continued to carry load after the RH upper longeron severed, but the fatigue test was halted at 55,100 cycles in order to conduct a teardown examination of the test article with the known fatigue failures.

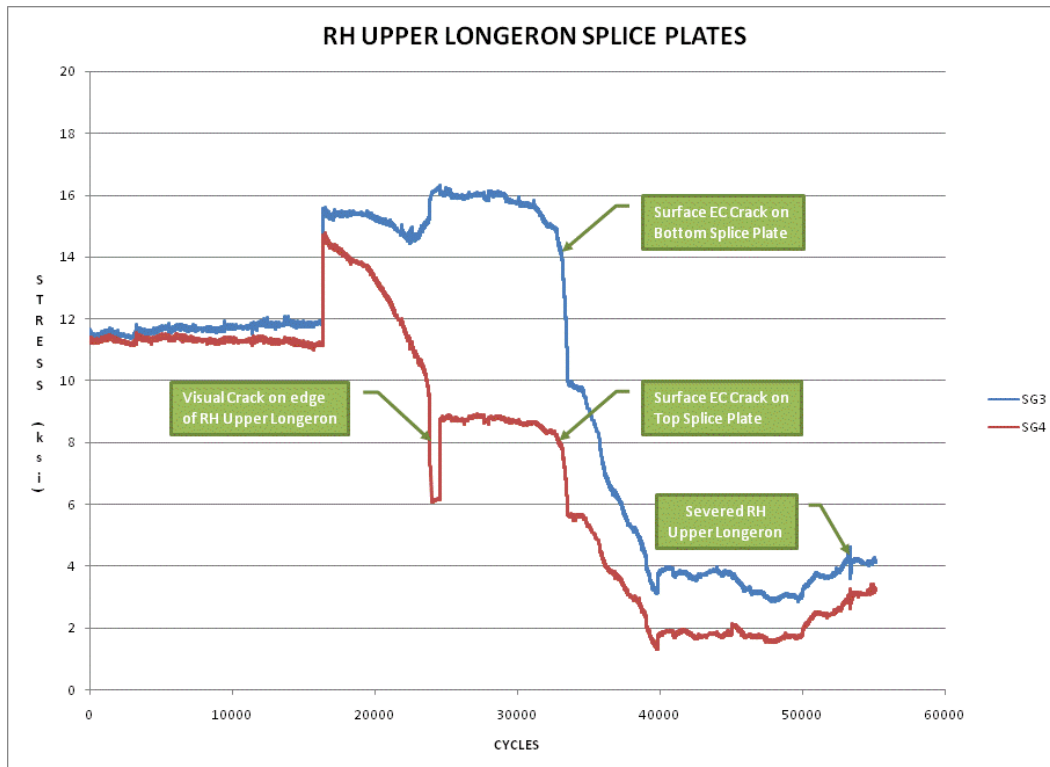


Figure 24: Loads Monitoring of Splice Plates on RH Upper Longeron

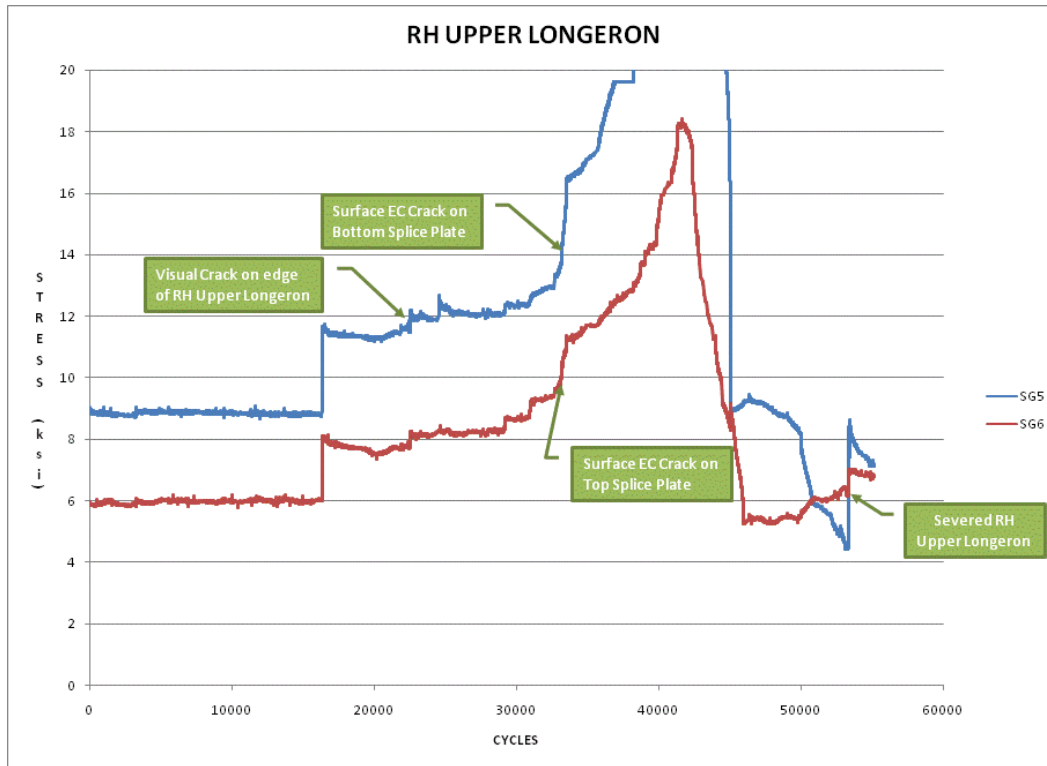


Figure 25: Loads Monitoring of RH Upper Longeron

6. VALIDATION AND ASSESSMENT OF SYSTEM DESIGN

In order to validate and assess the design of the SHIM system, researchers conducted a comprehensive teardown examination of the test article, and they correlated crack growth data from the teardown examination with sensor reading and crack growth prediction models. The correlation allowed researchers to validate the sensing technology for detecting cracks and monitoring crack growth. Using the data correlation, researchers were also able to assess capabilities of the SHIM system for predicting the remaining useful life and likelihood of structural failure. These predictions were based on interpretation of the sensor and analytical data along with assumed future operating conditions.

6.1 Test Setup

The teardown examination focused on the fatigue cracks located in the RH upper longeron. As illustrated in Figure 26, two cracks were located at the inboard fastener location just aft of the longeron splice on the upper and lower splice plates. Another crack, which

eventually led to fatigue failure, was in the original longeron portion, and it nucleated at the end fastener of the splice.

The RH upper longeron was extracted from the test article, as photographed in Figure 27(a), and further disassembled for examination, as photographed in Figure 27(b). Optical stereomicroscopy and scanning electron microscopy examinations were conducted on three fractures, which are photographed in Figure 28. Fracture #1 is the one fracture that nucleated in the original RH upper longeron at the aft end fastener common with the splice plates (#1A) and propagated through three other fastener locations (#1B, #1C, and #1D) prior to severing the RH upper longeron. Fastener location 1C, which cannot be seen in the photograph, is located in the upper flange of the RH upper longeron just above the leg of the longeron T-section. Fracture #2 is in the lower splice plate, and Fracture #3 is in the upper splice plate. As photographed in the close-up views in Figure 29, both of these fractures propagated from the inboard fastener location just aft of the splice to the inboard edge of the splice plate.

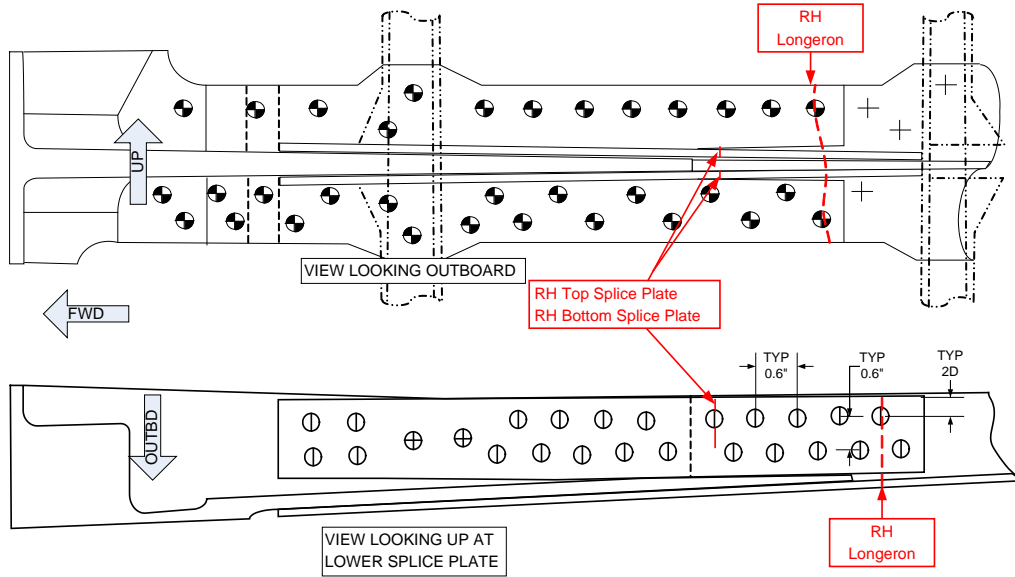
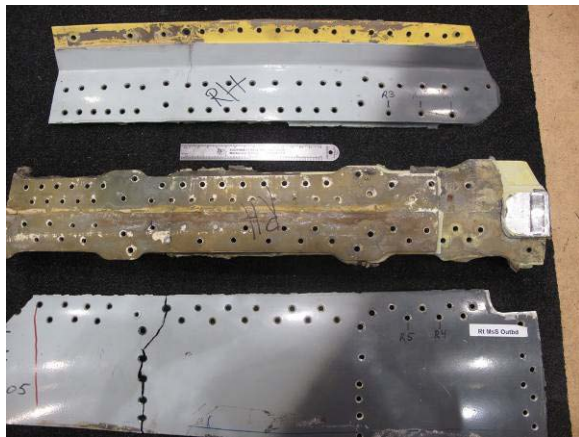


Figure 26: Fatigue Crack Locations in RH Upper Longeron



a) Extraction

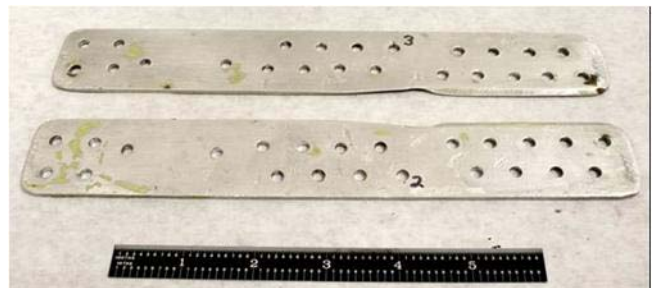


b) Disassembly

Figure 27: Extraction and Disassembly of RH Upper Longeron



a) Fracture #1

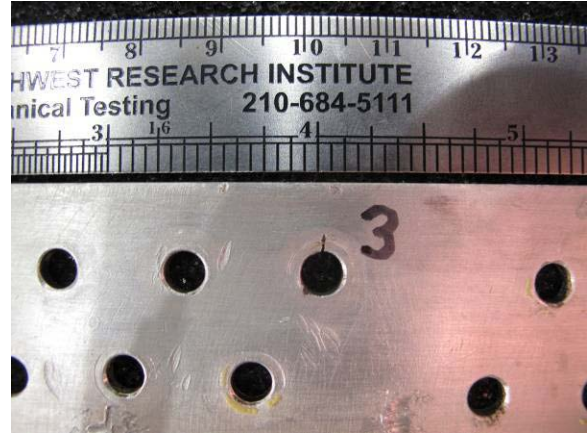


b) Fractures #2 and #3

Figure 28: Fractures in RH Upper Longeron



a) Fracture #2



b) Fracture #3

Figure 29: Close-up Photographs of Fractures #2 and #3

While the microscopy examinations measured distance of marker bands and locations of striation counts in each of the three fractures, Fracture #3 provided measured crack growth data that could be correlated to sensor readings and crack growth analyses. Eighteen marker bands were observed in Fracture #3. Two additional probable locations of marker bands were identified in Fracture #3, but these two locations could not be confirmed in the microscopy examination. The observations on Fracture #3 indicate stable crack growth at the FCL during fatigue testing. Table 1 summarizes the distances of marker bands measured in Fracture #3 during the teardown examination.

Table 1: Identified Marker Band Distances from Fracture #3 Origin in Upper Splice Plate of RH Upper Longeron

Marker Band	Distance from Origin (inches)	Marker Band	Distance from Origin (inches)
10	0.0018	4	0.0139
4	0.0031	6	0.0157
6	0.0040	10	0.0179
10	0.0053	4	0.0198
4	0.0061	6	0.0220
6	0.0070	10	0.0334
10	0.0074	4	0.0430
4	0.0090	6*	0.0540
6	0.0109	10*	0.0787
10	0.0126	10	0.1226

*Note: At these two observations, marker bands are probable; however, they could not be confirmed.

6.2 Correlation of Sensor Data and Fatigue Test Results

Of the three locations monitored on each upper longeron during the fatigue test, two fatigue cracks were identified on the upper and lower splice plates of the RH upper longeron. An additional fatigue crack was identified in the RH upper longeron at the aft fastener location common to the splice plates, and this fatigue crack eventually led to the catastrophic failure of the RH upper longeron. However, this location was not initially monitored with MsS sensors since a fracture mechanic model of this location was not available for use during the research project. While subsequent monitoring and sensor readings of this location showed indications of crack growth, the lack of a fracture mechanics model prevented researchers from correlating sensor data with crack growth data at this aft location. Thus, for this location, resources were not available to provide the predictor portion of the calculations used in the SHIM reasoning algorithms.

The one location where all the pieces needed for calibrating the damage sensor system were present (sensor readings and fracture data along with a fracture mechanics model) was the upper splice plate on the RH upper longeron (Fracture #3). Therefore, sensor data and fatigue test results were correlated for this location. With this data correlation, researchers were able to establish a minimum detectable level for the MsS sensor monitoring of the upper longeron splice plate and determine the relationship between the sensor magnitude readings and flaw size. Figure 30 shows the correlation of crack growth analysis, fracture data, and sensor readings with cycle counts from the fatigue test.

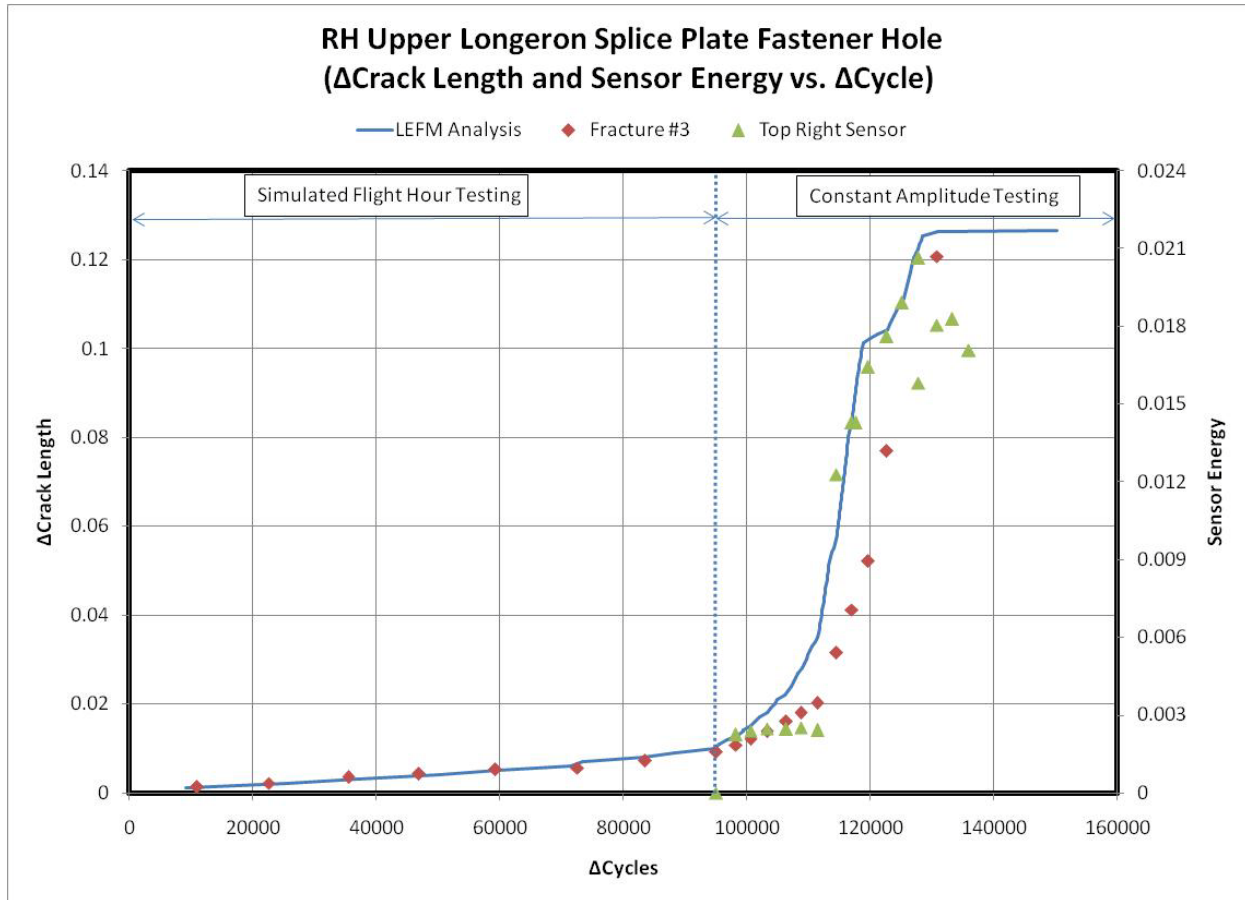


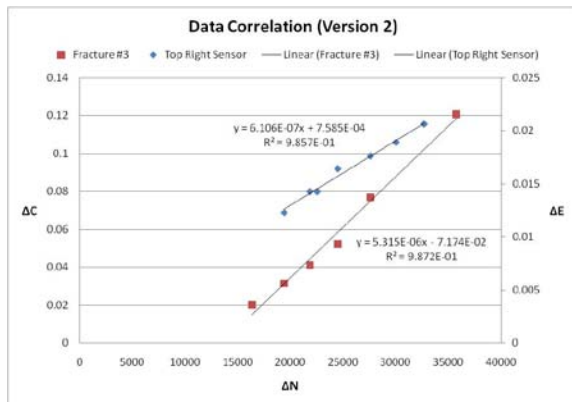
Figure 30: Correlation of Analysis, Fracture, and Sensor Data

Utilizing the strain gauge readings from the RH upper splice plate (SG4), a LEFM analysis was performed for the upper longeron splice plate. This analysis showed that stable crack growth occurred during the first 35,770 cycles of the constant amplitude testing, and then, the crack growth arrested when the stress levels at SG4 tapered off below about 5-ksi. By matching cycle counts from the fatigue test with marker bands observed in Fracture #3, it was determined that slow stable crack growth at Fracture #3 had actually started during the simulated flight spectrum testing. The crack growth rapidly increased during the initial portion of the constant amplitude testing until the stress levels at SG4 dramatically decreased, apparently due to loads redistribution from the crack propagating in the RH upper longeron at the aft end of the splice plates. This combined stress spectrum was used in the LEFM analysis, showing a close match between the analysis (solid blue line in Figure 30) and fractographic data on Fracture #3 (red diamond data points in Figure 30). Sensor energy readings (green triangle data points in Figure 30) were overlaid with the LEFM analysis and Fracture #3 data at the specified cycle counts where

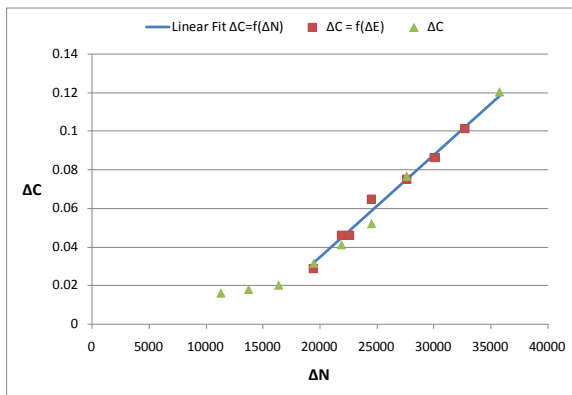
sensor readings were taken during the constant amplitude testing. This overlay showed an excellent correlation between sensor magnitude readings and flaw sizes for the region of rapid stable crack growth, which occurred between the cycle counts of 19,430 and 35,770 during the constant amplitude testing.

The correlation of sensor magnitude with flaw size focused on this region of rapid stable crack growth. As shown in Figure 31(a), the fractographic data (ΔC) and the sensor readings (ΔE) are plotted versus the cycle count (ΔN), and linear relationships were determined for ΔC and ΔE as a function of ΔN . Based on these two relationships, a relationship was defined for ΔC as a function of ΔE so that the flaw size could be estimated based on sensor readings. This relationship of $\Delta C = f(\Delta E)$ was defined about the mean flaw size, μ_C . The flaw size distribution based on sensor readings was calculated from the average difference, μ_d , between linear fit of $\Delta C = f(\Delta N)$ and $\Delta C = f(\Delta E)$. Assuming that sensor readings were normally distributed about μ_C , defined by the relationship of $\Delta C = f(\Delta E)$, the variance in the flaw size, σ_C^2 , was defined as μ_d^2 . This flaw size, μ_C , and its variance, σ_C^2 , was

used to estimate the flaw size distribution based on sensor readings. It is then combined with the predictions equivalent using the Bayesian updating algorithm discussed previously in Section 4 of this paper. Bayesian principles were applied in order to determine a weighted average flaw size distribution based on both analysis and sensor data. The weighted average flaw size distribution was then used to provide an improved estimate of the remaining useful life and probability of structural failure for the critical component. For the specific case of the RH upper longeron splice plate, correlation of the analysis and sensor data indicated that the minimum detectable level of crack growth was 0.045-inch with an average difference of 0.020-inch. Once crack growth exceeded the minimum detectable level, the accuracy of the sensor readings to estimate flaw size improved to an average difference of only 0.0055-inch. This improved accuracy is illustrated in Figure 31(b), showing how flaw sizes estimated based on sensor readings ($\Delta C = f(\Delta E)$) match up with fracture data (ΔC) and the linear fit of fracture data with cycle counts ($\Delta C = f(\Delta N)$).



a) Linear Fit of Sensor and Fracture Data



b) Relationship between Sensor and Flaw Size

Figure 31: Correlation of Sensor Magnitude with Flaw Size

Based on the data correlation, a minimum detectable level of 0.045-inch with a variance of 0.0004-inch² was used in the Bayesian updating, as described in Section 4, in order to assess the structural health and integrity of the upper longeron splice plate. As was shown in Figure 20 and discussed in Section 4.3.2, continual monitoring of the upper longeron and updating of flaw sizes based on analytical and sensor data improved the fatigue life prediction of this critical structural component by at least a factor of two. Figure 21 in Section 4.3.2 also illustrated how the likelihood of structural failure could be reduced through continual SHIM. However, since researchers were not able to continue the SFH testing until fatigue failure of the splice plates, they were not able to complete a comprehensive assessment of the SHIM system.

7. CONCLUSION

This applied research project achieved its objective of investigating the feasibility of integrating damage sensor technology with current methodologies used for usage monitoring and failure analysis. This integration would lead to a SHIM system for critical airframe components. The internal R&D project demonstrated the viability of integrating remote sensing for structural flaw nucleation and growth with intelligent reasoning logic and algorithms. This integration permits discernment in the health and integrity of a complicated structural component under realistic loading. Specific accomplishments and observations in each of the project tasks are summarized below.

Characterization of Failure Modes

- Fatigue failure modes were characterized for the upper longeron, a critical structural component of a jet trainer aircraft.
- Structural system reliability analysis appropriately identified four specific critical fastener locations where failure would likely occur, confirming results of previous DTAs and full-scale fuselage fatigue test along with identifying the location where final fracture did occur.
- Conventional DTA was conservative in estimating the structural fatigue life of the upper longeron.

Design of Damage Sensor System

- MsS sensors provided non-intrusive and remote means of monitoring and inspecting critical areas of a structural component.
- Review of sensor readings clearly identified flaws at two critical locations on the RH upper longeron – the upper splice plate and the original longeron itself at the aft fastener location common to the splice plates.

- Readings at other sensor locations were inconclusive due to insufficient data.

Component Level Reasoner

- Reasoning logic and algorithms were developed for assessing the structural health and integrity of the upper longeron.
- Bayesian principles were employed to integrate sensor data with crack growth analyses based on actual usage in order to provide an improved estimation of flaw size at critical locations.
- The reasoning logic and algorithms incorporated the improved estimation of flaw size into crack growth and probability of failure analyses in order to predict the remaining useful structural life and likelihood of structural failure for the critical component.

Component Testing of System Design

- Cyclic fatigue testing was conducted under both simulated severe flight spectrum loads and constant amplitude loads.
- The extensive number of cycles applied under the simulated flight spectrum testing highlighted the conservatism of the conventional DTAs previously conducted for the upper longeron.
- Loads monitoring of strain gages during the fatigue test quickly identified where structural loads were being shed and redistributed, leading to earlier detection of a flaw in the RH upper longeron. This flaw eventually led to catastrophic fatigue failure of that longeron.
- Application of marker bands during fatigue testing provided clear indications of crack growth with cycle counts in three separate fractures in the RH upper longeron.

Validation and Assessment of System Design

- Teardown examination of fractures in the RH upper longeron and its splice plates were essential to providing crack growth data for correlation with sensor data.
- Analysis of fractographic data, sensor data, and fracture mechanics models show good correlation between all three data sets at the upper splice plate on the RH upper longeron.
- The data correlation was key to establishing the minimum detectable flaw size for the MsS sensor and the accuracy of the sensor readings in order to estimate flaw size during rapid stable crack growth.

This research project validated the achievability of using a SHIM system to continually monitor and assess the health and integrity of critical structural

components. Implementation of a SHIM system has the potential to reduce the likelihood of structural failure and increase maintenance effectiveness, thereby reducing maintenance costs for complicated structural components in inaccessible areas. However, several areas should still be addressed in order to implement the sensor technology and structural assessment methodology developed under this research project on actual aircraft.

- A new sensor probe design with internal biasing capability may yield better results. For example, the new design could generate a DC biasing field through an electronic designed low profile DC coil coupled to the MsS transmission/receive coil rather than using fixed biasing magnets.
- Current MsS software needs additional modification in order to detect small changes associated with crack growth monitoring.
- An efficient and effective means needs to be developed for conducting fatigue tests of critical structural components in order to correlate crack growth data and sensor data, an essential part of establishing the probability of detection and accuracy of the damage sensor system.
- The reasoning process needs to be automated for known FCLs in order to conduct assessments of a critical component's structural health and integrity in a timely manner.

ACKNOWLEDGMENT

The authors of this report wish to express their appreciation to Andrea Moreno, Dr. Kenneth Griffin, Dr. Hal Burnside, Dr. Ronghua Wei, the Institute's Advisory Committee for Research, the T-38 System Program Office at Hill Air Force Base (AFB), and maintenance personnel at Randolph AFB for their contributions to this research project.

NOMENCLATURE

a	flaw size
ASIP	Aircraft Structural Integrity Program
CDF	cumulative density function
DTA	damage tolerance analysis
FCL	fatigue critical location
FSD	flaw size distribution
FORM	First Order Reliability Method
LEFM	linear elastic fracture mechanics
LH	left hand
MCS	Monte Carlo simulation
MsS	magnetostrictive sensor
NDI	nondestructive inspection
Nz	vertical acceleration
POF	probability of failure
RH	right hand
SG	strain gauge
SFH	simulated flight hours

SHIM	structural health and integrity monitoring
f	marginal probability density function
c	random variable representing crack size
z^*	measurement value of the crack size
a	normalization term
ΔC	fracture data
ΔE	sensor energy readings
ΔN	cycle count
μ	mean
σ^2	variance

REFERENCES

- (Aeronautics Science and Technology Subcommittee, 2007) Aeronautics Science and Technology Subcommittee, *National Plan for Aeronautics Research and Development and Related Infrastructure*, Committee on Technology, National Science and Technology Council, 2007.
- (Burnside et al., 2007) H. Burnside, et al. *T-38 Fuselage Structural Life Evaluation, Phase 4, T-38 Fuselage Life Evaluation*, Final Report, SwRI Project No. 18.05808, 2007.
- (Department of Defense, 2005) Department of Defense Standard Practice. *Aircraft Structural Integrity Program (ASIP)*, MIL-STD-1530C (USAF), 2005.
- (Derriso, 2008) M. Derriso. *Effective State Awareness Information is Enabling for System Prognosis*, Presentation at Workshop on Prognosis of Aircraft and Space Devices, Components, and Systems, 2008.
- (Domyancic et al., 2009) L. Domyancic, et al. *A Fast First-Order Method for Filtering Limit States*, 50th AIAA/ASME/ASCE/AHS/ASC Structures, Structural Dynamics, and Materials Conference, 2009.
- (Gallagher, 2007) J. Gallagher, et al. *Demonstrating the Effectiveness of an Inspection System to Detect Cracks in Safety of Flight Structure*, Presentation at 10th Joint DOD/NASA/FAA Conference on Aging Aircraft, 2007.
- (Giurgiutiu, 2007) V. Giurgiutiu. *Damage Assessment of Structures – an Air Force Office of Scientific Research Structural Mechanics Perspective*, Key Engineering Materials, Vol. 347, pp 69-74, 2007.
- (Hatcher, 2007) W. M. Hatcher. *21st Century Logistics: Reaching the Goal*, Presentation at 10th Joint DOD/NASA/FAA Conference on Aging Aircraft, 2007.
- (Hudak et al., 2006) S. J. Hudak, Jr, et al. *Embedded Thin-Film Sensor for Crack Detection and Monitoring in Fracture Critical Turbine Engine Components*, Proceedings of ASME Turbo Expo 2006, May 8-11, 2006.
- (Hudak et al., 2007) S. Hudak, et al. *Enabling Life Prediction, Sensing and Probabilistic Analysis*

- Technologies for Enhanced Engine Health Management*, Presentation at Integrated System Health Management Conference, 2007.
- (Roach, 2007) D. Roach. *Smart Aircraft Structures – A Future Necessity*, Article in High Performance Composites, 2007.
- (Smith et al., 2008) L. Smith, et al. *Conditional Filtering for Simplification of Aircraft Structural System Reliability Calculation*, 49th AIAA/ASME/ASCE/AHS/ASC Structures, Structural Dynamics, and Materials Conference, 2008.
- (Thwing et al., 2010) C. Thwing, et al. *The Use of Magnetostrictive Sensor Technology for Structural Health Monitoring*, Presentation at Aircraft Airworthiness and Sustainment Conference, 2010
- (Wieland, 2005) D. Wieland. *T-38 Longeron Splice Fine Mesh Model Integration*, Final Report, SwRI Project No. 18.08674, 2005.
- (Wieland et al., 2009) D. Wieland, et al. *T-38 Aircraft Structural Integrity Program Serp Support Tasks: FY08, Durability and Damage Tolerance Analysis*, Final Report, SwRI Project No. 18.12457, 2009.
- (Wignall, 2007) W. Wignall, Col. “*Executive Summary, Aircraft Accident Investigation, F-15C, T/N 80-0034*,” Lambert Field IAP, Missouri, 2007.

Dale A. Cope is a program manager in the Aerospace Structures section at Southwest Research Institute. A retired Air Force officer with over twenty years experience in aircraft structures, Dale has worked as an aerospace engineer, university professor, and aircraft maintenance officer. His engineering experience spans the fields of design, liaison, and structural analysis. He actively works in the research area of aircraft structural integrity, having performed airworthiness evaluations on civilian and military aircraft ranging from general aviation commuter airplanes to large military transport and bomber aircraft. Dale is currently investigating methods for integrating remote sensor technology with probabilistic structural failure analysis through intelligent reasoning algorithms in order to assess the likelihood of structural failure.

- PhD in Aerospace Engineering, Wichita State University, Wichita, KS, USA, 2002
- MS in Aeronautical Engineering, Air Force Institute of Technology, Wright-Patterson AFB, OH, USA, 1988
- BS in Aerospace Engineering, Texas A&M University, College Station, TX, 1982
- Senior member of American Institute for Aeronautics and Astronautics